Thesis for The Degree of Licentiate of Engineering

Investigating Lithium-Ion Battery Electrode/Electrolyte Interfaces using Ambient-Pressure X-ray Photoelectron Spectroscopy

Sofia Reiner

Department of Physics and Astronomy

Chalmers University of Technology

Gothenburg, Sweden, 2026

Investigating Lithium-Ion Battery Electrode/Electrolyte Interfaces using Ambient-Pressure X-ray Photoelectron Spectroscopy

Sofia Reiner

Department of Physics and Astronomy

Chalmers University of Technology

SE-412 96 Göteborg,

Sweden

Phone: +46(0)31 772 1000

Cover: The measurement chamber at the HIPPIE beamline at MAXIV, Lund, with the author's hands refilling the electrolyte beaker of the electrochemical cell. Photo taken by Julia Maibach.

Printed by Chalmers Digitaltryck,

Gothenburg, Sweden 2026.

Investigating Lithium-Ion Battery Electrode/Electrolyte Interfaces using Ambient-Pressure X-ray Photoelectron Spectroscopy

Sofia Reiner

Department of Physics and Astronomy
Chalmers University of Technology

Abstract

Rechargeable batteries store and release energy through interfacial electrochemical reactions, making interfaces central to battery performance, lifetime, and safety. In lithium-ion batteries, the solid electrolyte interphase (SEI) formed between the electrode and electrolyte is essential for stable operation. The SEI is chemically and structurally heterogeneous, participates in lithium-ion transport, may evolve during battery operation and appear to host a permanent electric potential gradient. However, many of its kinetic characteristics remain poorly understood, largely due to the experimental challenges associated with probing buried interfaces between the battery materials under operation. This thesis addresses these challenges by combining well-defined model systems with operando ambient-pressure X-ray photoelectron spectroscopy (APXPS). By probing the bulk electrolyte meniscus rather than the buried interface directly, SEI-related processes can be investigated under working conditions. An electrochemical test protocol exploiting the self-discharge and relaxation of the electric double layer at the interface is introduced, expanding on existing electrochemical models used with APXPS, to also capture information about the SEI. This approach enables identifying the SEI onset and provides insight into surface reaction kinetics. Additionally, *in situ* and *operando* experimental approaches are compared, clarifying what interfacial information can be extracted from each and outlining their respective advantages and limitations. Together, these results contribute to a deeper understanding of SEI formation and interfacial dynamics in lithium-ion batteries.

Keywords: lithium-ion battery, battery interfaces, solid electrolyte interface, electrochemical potential, ambient-pressure photoelectron spectroscopy, operando, in situ

List of Papers

This thesis is based on the following papers:

I **S. Reiner**, I. Källquist, I. Bengtsson, A.O. Elvarsson, I. Drevander, R. Temperton, J. Halldin Stenlid, P. Johansson and J. Maibach,
Studying Relaxation Effects across Battery Electrode/Electrolyte Interfaces using Ambient-Pressure X-ray Photoelectron Spectroscopy
In manuscript.

II **S. Reiner**, A.O. Elvarsson, G. Middendorf, S. Dovrén, I. Drevander, H. Andersson, R. Temperton and J. Maibach,
Comparing In Situ and Operando Dip-and-Pull Ambient-Pressure X-ray Photoelectron Spectroscopy using Model Battery Systems
In manuscript.

Contribution Report

Paper 1:

SR and JM planned the experiment and SR prepared samples. SR, JM, AOE, ID, RT performed the synchrotron experiments. SR performed the data analysis and IB contributed to the peak fitting algorithms. JHS, PJ and IK participated in discussions and data interpretation. SR wrote the manuscript with input and editing from JM.

Paper 2:

SR and JM planned the experiment. SR prepared all samples except for the LFP reference electrode which was done by GM under the supervision of SR. SR, JM, AOE, GM, SD, HA, IS and RT performed the synchrotron experiments. SR performed the data analysis and wrote the manuscript with input and editing from JM.

Contents

Chapter 1
Introduction

Rechargeable batteries can convert electrical energy into chemical energy during charging, and the process can be reversed to release energy when needed during discharge. The chemical reactions governing this energy conversion take place at the interfaces between electrodes, which conducts electrons, and electrolyte, conducting ions. Here, the charged particles can meet, and through the addition of electrical energy, form new chemical species or structures, changing the chemical potential of the battery. While simple in theory, more often that not, multiple chemical pathways exists at the interface, creating a complex network of reactions, some of which may not be reversible in nature. This means that the interfaces of the battery are constantly evolving as the battery is operated and used. Because of this, a battery's performance, lifetime and safety are closely linked to its interfaces. Understanding how they are evolving is therefore of great interest both for existing technologies but also for next generation batteries.

As of 2026, the year of this thesis, the lithium-based battery is still the most widely used battery technology in the world, largely because of its high energy density and efficiency. The success of lithium in the world of energy storage can be traced to its very high affinity to give electrons to other species, the highest of any solid elements in the periodic table [1]. This makes lithium an ideal material to use when building a battery, which relies on the movement of electrons. It, however, also leaves lithium highly reactive to most types of materials, making it difficult to work with, especially if only one type of reaction is coveted. The operation of the battery is therefore dependent on the formation of the solid electrolyte interphase (SEI), an interphasial layer between the electrode and the liquid electrolyte. While it in early studies of the LIB system was shown to stem from unintentional side reactions [2], it has proven to be the key to lithium-based batteries working stably. Despite being a highly studied part of the battery some of its characteristics, connected to both kinetics and chemical composition, remains unresolved. Contrary to many oxide layers forming on metal electrodes, the SEI is not just a passivating film, but participates in the movement of positively charged ions across the interfaces of the battery. Furthermore, the layer is typically heterogenous, with some parts being more compact and other porous. The makeup of the SEI is dependant on the battery materials themselves and its characteristics such as chemical composition, thickness and conductivity may also change as the battery is operated [3–5]. Interestingly, it has also been shown to contain some type of static electric field, potentially generated from the gathering of charged species in the interphase [6, 7]. The profile, strength and origins of this field has, however, been rarely described.

A reason for the lack of insight into the dynamics of the SEI is because they are so cumbersome to unambiguously study. The SEI lies sandwiched between two dense phases and a straightforward approach would perhaps be to simply

separate the materials and probe the exposed surfaces directly. This introduces a number of problems. Most characterisation techniques, especially those requiring ultra-high vacuum, can alter or destroy the very species they aim to observe. Once the battery is disassembled or exposed to vacuum, liquid species may evaporate. Additionally, many interfacial reactions occur only under operating conditions when all battery materials are in contact and under external bias, for example an applied voltage. Even techniques designed to probe batteries under conditions close to real operation suffer from inherent limitations. These include the need for specialised cell designs, weak signals, or signals that are a convolution of multiple simultaneous processes. In the case of X-ray-based methods, beam-induced damage to the samples can further complicate interpretation. These challenges are particularly pronounced for the SEI, which is typically tens of nanometers thick and therefore requires both high interfacial sensitivity and careful control of the probing conditions.

One way to address some of these complications is to simplify the battery itself by using a model system. This allows to isolate specific reactions and phenomena that would otherwise be hidden by the complexity of the battery materials. Real batteries rarely contain single phase materials but components, such as the electrodes, instead contain a mixture of, for example, oxides, polymers and metals. No surfaces are perfectly flat and no bulk is homogenous, and while this typically makes for a functioning battery, they make fundamental studies more difficult since many variables change at once. In contrast, well-defined model systems allow for the study of a smaller subset of reactions and in a more controlled setting. While not exactly equalling the reactions of a battery they help to build a fundamental understanding that can thereafter be applied to a real life battery system.

Alongside choosing a simpler system, another strategy to overcome the challenges of studying the SEI is to use characterisation techniques such as ambient-pressure X-ray photoelectron spectroscopy (APXPS). Conventional XPS requires ultra-high vacuum which is incompatible with the liquid electrolytes present in LIBs. In contrast, APXPS is performed at slightly higher pressure, meaning some electrolytes can be introduced into the measurement chamber. Analogous to regular XPS, APXPS is a surface sensitive technique that can not only identify atomic species but also information about their chemical state, such as their surrounding atoms and oxidation state. While powerful, the limited probing depth means that probing the SEI directly is still challenging. To work around this limitation, previous studies have shown that bulk-sensitive measurements can be used to infer about some of the reactions at the interface between electrode and electrolyte [8, 9]. These methods, however, have not yet been able to resolve reactions associated with the SEI.

Addressing this gap, this thesis demonstrates that SEI formation can be identified by probing the bulk meniscus using APXPS. A cycling approach is introduced, using the relaxation and self-discharging of the electric double layer, to extend existing electrochemical models combined with APXPS to explicitly include SEI formation. This method enables to identify the onset of SEI growth and provides insight into the kinetics of surface processes. In addition, this work compares

different operational modes in APXPS measurements on model battery interfaces, highlighting what information can be extracted from from *in situ* versus *operando* measurements and discussing their respective advantages and limitations.

Chapter 2
Electrode/electrolyte interfaces

Without electrode/electrolyte interfaces there would simply be no batteries, and it is the presence of these interfaces that defines electrochemistry as a subfield of chemistry. The spontaneous reactions between chemical species in the electrode and the electrolyte release heat due to the lowering of the Gibbs free energy of the system. When an additional electrode is introduced in the electrolyte, it instead allows to divert electrons through an external circuit and what was previously released as heat will now be in the form of electrical energy, a current, which can be directed and used. Using two electrodes also makes it possible to apply an external electric potential, driving non-spontaneous reactions in a controlled manner and forming new species on the electrode [10]. Electrochemistry therefore encompasses not only batteries but also the disciplines of catalysis, electrolysis and electrodeposition. It is an extensive discipline and at its core lies the interactions between electrode and electrolyte. This chapter will introduce the fundamental principles of the interface with particular emphasis on electric potentials close to the interface and the mechanisms enabling charge transfer across it. These principles provide the theoretical basis required to understand how interphases, particularly the SEI, form on battery materials and why their formation is central to the performance, stability, and lifetime of electrochemical energy-storage devices

2.1 The bulk electrolyte

Before introducing electrodes, it is useful to first examine the bulk electrolyte, the transport of charge in it, and the carriers' interactions in the absence of an applied external field. An electrolyte is by definition a medium which is non-conducting to electrons but conducting to ions, both positively charged *cations* and negatively charged *anions*. This being the basic condition, the electrolyte needs to be able to release these species from their neutral state and make them available as charged ions. Electrolytes can be grouped into several categories depending on how they accomplish this. While *ionic liquids* and *solid-state electrolytes* are two of these categories, this thesis will focus on electrolytes where a salt is dissolved in a liquid solvent, thereby releasing the cations and anions in the salt from their ionic bond. Electrolytes of this kind are standard in commercial Li-ion battery systems and the ones that will be used in the experiments of this thesis [1, 11].

2.1.1 Solvation of salts

What constitutes a good solvent is its ability to quickly dissociate the cations and anions from each other. A solvent molecule with a high dipole moment is typically more successful at this as the end of the molecule with a higher positive charge density will orient itself against the anion, and similarly the part of the molecule with higher negative charge density against the cathode. The solvent molecules arrange themselves around each ion, forming a stabilizing "shield". Closer to the

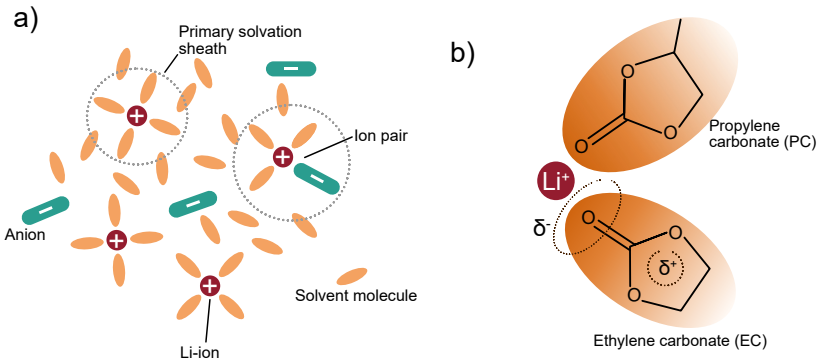

Figure 2.1: a) Solvation of a lithium salt, illustrating the preferential orientation of solvent molecules around the Li^+ ion (red circle), while contact ion pairs may also form between cations and anions (green beans). b) Solvation structure of ethylene carbonate (EC) and propylene carbonate (PC), showing that the positive terminus of the molecular dipole is shielded within the carbon ring

ion, which can be idealized as a point charge with a Coulombic potential, the electric field is strong enough to align the dipoles of nearby solvent molecules. As the distance from the ion increases, the field weakens, and the dipoles eventually adopt random orientations. The region in which the solvent molecules remain oriented by the ion's field is referred to as the *solvation sheath* (Figure 2.1a). Only the dipoles closest to the ion will follow along when the ion moves in the bulk electrolyte. These are said to belong to the *primary solvation sheath* and the average number of solvent molecules in this sheath is the *solvation number* of the electrolyte [1, 12].

A high dipole moment, however, does not automatically mean that the solvent is better at solvating all salts and their ions. The solvation will also depend on the distribution of the positive and negative charge centres in the molecule. If, for example, the centre of the positive charge δ^+ is located within the structure of the molecule it may not be as accessible to the anions as the negative pole δ^- is to the cations, as seen in Figure 2.1b. This is for example the case for the cyclic carbonates ethylene carbonate (EC) and propylene carbonate (PC), where the positive pole is located in the carbon-ester ring. As a consequence these solvents will solvate the cation more than the anion [1]. In the case of LIBs, lithium salts are used, where a Li^+ cation is paired with various types of anions. Organic solvents, such as PC, EC or linear carbonate esters are typically used as solvents, all of which solvate the cation better than the anion [11, 13, 14]. Furthermore, as will be discussed further on, it is the solvation sheath of Li^+ that plays the greatest role on the formation and chemistry of the interphases formed between electrode and electrolyte.

Finally, it should be said that the model presented above is only accurate if there is enough solvent molecules to fill the primary sheath. If not, the Coulombic

potential of the ions will not be screened and they will feel the field of each other. This can lead to the formation of *ion pairs*, which can be seen as a middle step between fully solvated ions and neutral salt crystals [1]. At which concentration the ion-pair interactions start to dominate over the cation-solvent interactions will depend on the salt and solvent themselves. In this work, no lithium salt concentrations above 1 M (mole/litre) have been used. Both computational and experimental studies generally agree that, at this salt concentration in non-aqueous electrolytes, solvent–ion interactions dominate; however, the ions are not fully screened [11, 15].

2.2 Introducing an electrode

In the preceding section, the electrolyte has been assumed to behave as a homogeneous bulk phase, where ion–solvent interactions are isotropic so that the fields experienced by the solvent molecules and ions are the same in all directions. This symmetry can be broken by introducing an electrode into the liquid electrolyte. While the electrode could both be made up of only one material or phase, like a metal, or multiple components, like a typical battery electrode, the general structure is the same with fixed cation sites in the lattice and delocalised electrons belonging to the conduction band which are free to move around. They produce a very different local electric field to that of the electrolyte. Inserting an electrode into the electrolyte causes a spatial redistribution of charges in order to reach a new equilibrium between Coulombic fields. While some ions will be either attracted or repelled to the electrode, most ions in the electrolyte will not be considerably bothered by the new interface since they are far enough away to not feel the field of the electrons at the electrode surface. Therefore they will not reorganise themselves and a concentration gradient will only appear between the interface and the bulk. This is the formation of the *electric double layer* (EDL), a important component in electrochemistry that will affect both reactions and kinetics at the surface [1, 12].

2.2.1 A quick note on charge and potentials

In the electrode, any charge will be located on the surface [16]. While it later will be seen that the total net charge of the electrode can be both negative or positive depending on the direction of an externally applied voltage, for the recently introduced electrode it is still zero. As a result of the nature of the electrode and anisotropy of the interface, however, there will still be either a small accumulation or depletion of electrons on the surface [1]. For the sake of simplicity, in this and the following sections the surface of the electrode will be assumed to take on an excess of negative charges when introduced into the electrolyte.

So far the fields and potentials described have been Coulombic, coming from ions that were treated as point charges. The electrostatic potential ϕ can now instead be defined between two points as the integral of the electric field [12, 17, 18]. Before bringing the two phases together, $\phi = 0$ in both bulk phases, respectively. After dipping the electrode into the electrolyte, the redistribution of charges will cause an electrostatic potential gradient to form, with the difference in potential

between the two phases at the interface being $\Delta\phi = \phi^{electrolyte} - \phi^{electrode}$, and $\Delta\phi > 0$ if defined by the work needed to move a positive single charge. This value is called the *Galvani potential* or *inner potential difference* of the interface.

2.2.2 The models of the electric double layer

Studying the EDL can be divided into two parts: 1) determining the strength and capacity of the layer, or in other words the amount of excess charges at each side of the interface compared to the bulk and 2) the profile of the layer, in what way and how far the disruption causes reorganising of ions [12]. The former can be studied by the surface charge's relation to the surface tension of the electrolyte, a field called *electrocapillarity*. The second is harder to probe, mostly because the EDL in non-aqueous electrolyte is on the nanometer scale [17]. Therefore, the structure is understood by models that have been proposed, tested, rejected and reworked over the years, with no all-encompassing model existing to this day.

The earliest formulated model, the Helmholtz model (sometimes Helmholtz-Perrin), was introduced in the second half of the 19th century and treated the interface as a perfect capacitor in which the electrons and cations distributed themselves evenly on the two sides of the interface [19–21]. Arguing that due to thermal dynamics and the random movement of ions, there was no way for the ions to orderly stay on the surface, Gouy counter-proposed that the concentration of cation ions would instead diffuse from the electrode surface [22]. This eventually became the Gouy-Chapman theory which described the potential as decaying exponentially from the surface [23]. Stern thereafter suggested to combine the two models to cover both the case of concentrated electrolytes, where the ions tend to form a more compact capacitor-like layer, and diluted electrolytes where the layer is more spatially extended [12, 24]. Despite its improved accuracy over earlier models, the Stern model failed to explain why experimental results varied depending on the anion present. Grahame therefore proposed that certain anions can adsorb directly onto the electrode surface through short-range chemical interactions rather than purely electrostatic attraction, a process referred to as *specific adsorption* [25]. Because the mechanism anchoring the ion to the surface is not governed by the electrode charge, these ions may remain adsorbed even when their charge is identical to that of the electrode. The likelihood of a specific ion adsorbing is connected to the weakness of its solvation sheath, with poorly solvated anions being the most likely to adsorb to the surface [1]. The two-layer model was consequently split into three with the innermost layer of specifically adsorbed ions making up the *inner Helmholtz plane* (IHP), the ions closest to the electrode without losing their solvation sheath making up the *outer Helmholtz plane* (OHP) and finally the diffuse layer as described by the Gouy-Chapman model. In 1963 the latest significant change to the EDL model was made with Bockris, Devanathan and Müllen adding that solvent molecules may also be present in the IHP. In their work they argued that since the solvent molecules can orient themselves around the ions, they should be able to do the same to the electrode surface [26]. The solvent molecules' contribution to the potential across the interface was, however, deemed to be very small compared to the adsorbed ions. The BDM model can be seen in Figure 2.2a.

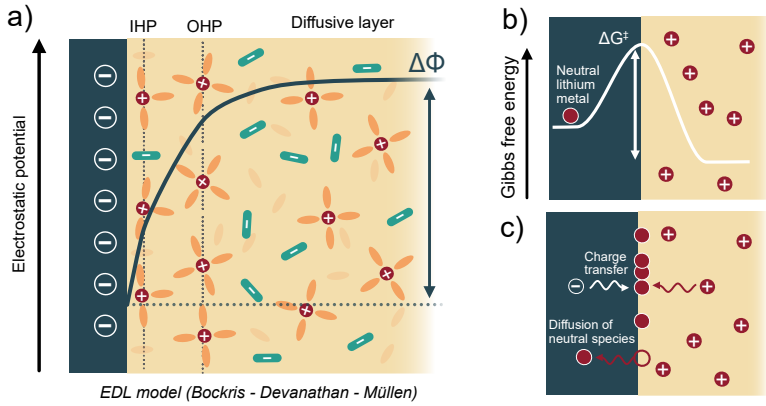

Figure 2.2: a) Formation of the electric double layer upon immersing an electrode in an electrolyte according to the Bockris–Devanathan–Müller (BDM) model. The inner Helmholtz plane (IHP) contains desolvated cations and may also include specifically adsorbed anions, while the outer Helmholtz plane (OHP) passes through the first layer of fully solvated cations followed by a diffuse layer. b) Schematic representation of the Gibbs free energy activation barrier that must be overcome for charge transfer to occur. c) Charge transfer reaction resulting in the deposition of neutral atoms on the electrode surface, followed by possible diffusion of these atoms into the electrode bulk as a secondary step.

These models together take into account the electrostatic interactions between solvent and ions, ions and electrode, and solvent and electrode, the specific adsorption to the surface of the electrode and the thermal dynamics of the bulk electrolyte. The models were, however, all proposed and tested for aqueous electrolytes, many of them dilute. Unlike EC and PC, in water, both poles of the dipole moment on the molecule are readily accessible to surrounding solute species, whereas in carbonate solvents the negative pole is more exposed, leading to inherently different solvation environments. This difference can significantly alter both the solvation mechanisms and the resulting structure of the electrical double layer. In addition, more weakly solvated anions in non-aqueous electrolytes promote ion-pair formation, an effect that is not adequately described by existing EDL models and has been shown to be significant in both experimental and computational studies [27–30]. The EDL models should therefore be treated more like a starting point than an absolute truth when discussing electrode/electrolyte interfaces.

2.2.3 Charge transfer at the interface

But what about reactions at the interface? The electrolyte can not accept free electrons and the electrode can not house the solvated ions, but it is not unthinkable that redox reactions could occur involving the delocalised electrons in the electrode and chemical species in the IHP and OHP regions of the EDL. Multiple electron pathways are theoretically possible, with one or more electrons

either being supplied or accepted by the electrode. The former is possible with the reduction of the cation, resulting in a neutral atom which is deposited on the surface of the electrode (Figure 2.2c). In the reverse process, the atom is oxidised and the cation released into the electrolyte. These two are the simplest examples of a *charge transfer* process which involves a charge being moved from one side of the interface to the other. Partial reduction or oxidation of the ions in the electrolyte, is also possible for some electrode/electrolyte systems, and would mean the ion remains in the electrolyte, although with a changed oxidation state. This is however not relevant in the topic of LIBs since Li^+ is very reluctant to loose another electron [1, 12, 17]. Furthermore, the cases discussed above consider only the reduction of the cation; however, since solvent molecules are also present at the IHP, they are naturally also susceptible to reduction. Later in chapter 3 it will be shown that on LIB electrodes the reduction of Li^+ and the solvent molecules can have a joint reduction pathway, resulting in the formation of the SEI briefly mentioned in the beginning of the thesis.

Returning to the general electrode/electrolyte interface, attention is now directed toward the factors governing the reactions in the first place. Reactions proceed only when they lead to a reduction in Gibbs free energy. However, reducing the Gibbs free energy is typically associated with some activation energy barrier $\Delta G^\ddagger$ which needs to be overcome (Figure 2.2b). The rate of the chemical reaction ν is given by

$$\nu = c\frac{k_B T}{h} e^{\frac{\Delta G^\ddagger}{RT}} \tag{2.1}$$

where c denotes the bulk concentration of the oxidising or reducing species [12, 17]. This is a simple chemical rate equation which only takes into account the thermodynamics of the reaction. The activation barrier will also be affected by the EDL close to the surface which may either aid in overcoming the barrier or hinder it depending on the work it performs on the involved ions in the electrolyte [1]. Furthermore, $\Delta G^\ddagger$ will typically not be equal for the corresponding redox reactions meaning one reaction will occur at a higher rate, depleting the reactants near the surface and changing the EDL. This will in turn counteract the previously favoured reaction until an equilibrium has been reached. This equilibrium does not necessarily mean no reactions are happening at the interface, but only that the rates of the redox reactions are balanced and the net current is zero.

2.2.3.1 Some additional definitions

The above described redox reactions all depend on the charge transfer of the electron at the surface. A distinction can be made between these processes and the adsorption and desorption of species at the electrode surface, for example as a result of the EDL forming. Since the former results in a charge transfer and therefore current across the interface, they are called *Faradaic processes* with the latter simply being *non-Faradaic processes* [12, 17]. They are often used to distinguish between reactions happening across the interface and the pure capacitive charging of the EDL.

Two other frequently occurring terms are the *ideal polarisable electrode* and

ideal non-polarisable electrode and while there are no real-life electrodes fulfilling the requirements of being ideal, they can still be used to describe the general behaviour in certain voltage ranges. An ideal polarisable electrode describes an interface where there is an infinite resistance to charge transfer, and therefore only charging of the EDL and non-Faradaic processes occur. Contrarily, the NPE has an infinitely low resistance to charge transfer reactions happening across the interface [12, 17]. A real life-electrode may function as a polarisable electrode in a specific voltage region since where there is no energy available to overcome the $\Delta G^{\ddagger}$ of the reactions. With an externally applied voltage, however, the electrode potential may be brought above the barrier to allow a reaction to occur. This is the workings of the electrochemical cell.

2.3 The electrochemical cell

After closely discussing the potentials forming at one electrode in an electrolyte it is clear that these two alone do not make a battery. There is no way to control or change the direction of chemical reactions at the electrode surface and concurrently, without an external circuit there is no means to utilise the current in an application. Therefore, another electrode needs to be introduced into the electrolyte. This electrode will naturally create an EDL of its own with a Galvani potential across the interface. Connecting two electrodes to form an *electrochemical cell* may result in a spontaneous current if it lowers the Gibbs free energy of the entire cell, this being called a *galvanic cell*. Using a *potentiostat* it is also possible to force transfer between electrodes, changing the potential and forcing the cell to increase the total Gibbs free energy. This is instead an *electrolytic cell* [10, 17]. A rechargeable battery is therefore a device made up of at least one electrochemical cell and it will operate both as a galvanic and an electrolyte cell depending on if the battery is being discharged or charged, respectively.

2.3.1 The electrochemical potential model

In order to discuss the direction of current and potential fields in the full cell, consisting of two electrodes in the electrolyte, without having to describe the thermodynamic states of all involved species and the Coulombic forces between them, it is useful to use a more macroscopic model. While there are multiple ways to organise such a model, here one will be presented that divides the electrochemical potential into a short range chemical contribution and a long range electrostatic contribution. Such a decomposition will prove to be especially useful when the model is combined with the XPS techniques of this thesis.

The electrochemical potential $\bar{\mu}$ of a species j in a phase α, is the work needed to add such a species to that phase from a reference point, which can be in another phase. It is given by:

$$\bar{\mu}_j^{\alpha} = \mu_j^{\alpha} + z_j F \phi^{\alpha} \tag{2.2}$$

where μ_j^{α} is the chemical potential and ϕ^{α} the electrostatic potential, introduced

previously, with both referenced to the same reference phase. Depending on the charge of the particle z_j will take on a positive (cation) or a negative (anion) integer, and for the electron $z_j = -1$ [17, 18]. In this version of the equation, the Faraday constant F has the unit of C/mol and $\bar{\mu}_j^\alpha$ a unit of J/mol. As XPS instead deals with the energy unit of electron volt (eV), it is preferred to use here as well and the equation can instead be written simply [9],

$$\bar{\mu}_j^\alpha = \mu_j^\alpha + z_j \phi^\alpha \tag{2.3}$$

If a species is neutral then $z = 0$, $\bar{\mu}_j^\alpha = \mu_j^\alpha$ and the electrochemical potential will just be the chemical potential of the species. Furthermore, in a charge transfer reaction, for example Li^+gaining an electron to form metallic lithium Li, the respective electrochemical potentials of the involved species are related through

$$\bar{\mu}_{Li}^\alpha = \bar{\mu}_e^\alpha + \bar{\mu}_{Li^+}^\alpha. \tag{2.4}$$

It should be noted that dividing the electrochemical potential into chemical and electrostatic contributions is purely a concept and there is no way to experimentally separate the two contributions and measure them individually, without making assumptions about the system itself [18]. Additionally, the term *chemical potential* might feel a bit obscure. If one would zoom in on any species far enough it would be clear that all forces acting on it are Coulombic and therefore electrostatic in nature, at least on small time scales. It is, however, a variable defined to show the difference between the chemical nature of different species, neglecting the effects of the long range electric field and is therefore a function of the Gibbs free energy:

$$\mu_j^\alpha = \left(\frac{\partial G_{int}}{\partial n_j} \right)_{T,P,n_{j \neq i}}. \tag{2.5}$$

If temperature T, pressure P, and the concentration of other surrounding species n_i stay constant, the chemical potential is given by the change in the internal *chemical* Gibbs free energy G_{int} as a function of the change in concentration of the species. Another way to express the chemical potential is through:

$$\mu_j^\alpha = \mu_j^0 + RT \ln c_j \tag{2.6}$$

with c_j being the concentration of the species, R is the gas constant and μ_j^0 being a standard state of the species at a given temperature T and pressure. Here, for simplicity, the species in the solution is assumed to behave ideally, and therefore the concentration is used instead of the activity. Any difference in concentration, and therefore difference in chemical potential along an axis will lead to diffusion of a species j in accordance with Fick's law:

$$J_j^{diff} = -D_j \nabla c_j = -\frac{D_j c_j}{RT} \nabla \mu_j \tag{2.7}$$

where J_j^{diff} is the flux of the species j and D is the diffusion constant. Similarly, the flux of a charged particle due to a difference in the electrostatic potential, the migration, is given by:

$$J_j^{migr} = -\frac{D_j z_j c_j}{RT} \nabla \phi. \tag{2.8}$$

Combining the contributions from the diffusion and migration, the the *Nernst-Planck equation* emerges, which describes the total ion transport J of a charged species,

$$J_j = -\frac{D_j c_j}{RT}\nabla\mu_j - \frac{D_j z_j c_j}{RT}\nabla\phi = -\frac{D_j c_j}{RT}(\nabla\mu_j + z_j\nabla\phi) = -\frac{D_j c_j}{RT}\nabla\bar{\mu}_j \quad (2.9)$$

From this equation it becomes clear that the difference between electrochemical potentials will drive the transport of species in the cell and that a species experiences two simultaneous driving forces: a chemical force, due to differences in concentration, and an electrical force, due to differences in in electric potential [1, 17, 31]. A charged species in either electrode or electrolyte, will move towards a region of lower electrochemical potential until the concentration gradients weaken and charge redistribution builds opposing electric fields, reducing the net driving force until equilibrium or steady state is reached and the net flux J_j diminishes. While applicable on all electrochemical cells, the Nernst-Planck equation neglects ion-ion interactions, making it only exact for very diluted systems where the Coulombic fields do not significantly overlap [1]. It was previously discussed that at the electrolyte concentrations used in this thesis, solvent-ion interactions dominate. It is, however, important to note that the interactions of ion-pairs might alter the contributions of the two fluxes.

2.3.2 Cell potential and voltage

With an electrochemical potential $\bar{\mu}_j^{\alpha}$ defined, the driving force between two electrodes in an electrolyte can also be expressed. This is the *cell voltage* E_{cell} which will be expressed in V. Introducing multiple electrodes in the electrolyte, each electrode would also have its own electrode voltage measured against a chosen *reference electrode* (RE) and the electrode of interest in a system would typically be called the *working electrode* (WE). Since the charge carriers in the external circuit are electrons, the cell voltage of a two-electrode cell will be given by

$$E_{cell} = E_{WE} - E_{RE} = -\frac{(\bar{\mu}_e^{WE} - \bar{\mu}_e^{RE})}{e} \quad (2.10)$$

with e being the elementary charge [17, 18]. The negative sign in front of the electrochemical potentials is due to the definition of voltage being the work to move a *positive* charge through an electric field. In a three-electrode cell where an additional *counter electrode* (CE) has been introduced, the cell voltage would be calculated through

$$E_{cell} = -\frac{(\bar{\mu}_e^{WE} - \bar{\mu}_e^{RE}) - (\bar{\mu}_e^{CE} - \bar{\mu}_e^{RE})}{e} = -\frac{(\bar{\mu}_e^{WE} - \bar{\mu}_e^{CE})}{e}. \quad (2.11)$$

Applying a voltage to a cell is therefore the same as changing the electrochemical potential difference between the electrodes, which allows an electrolytic cell to operate. A potentiostat does this by injecting or removing charges on the CE [32]. At the same time the RE should preferably act like an IPE without any charge transfer across its surface so that its electrochemical potential stays unchanged. In case of a two-electrode cell, the CE must also double as a RE, meaning that

there will be no way of separating the WE and CE individual contributions to E_{cell}. In order to properly study the interactions of a specific electrode/electrolyte interface, preferably a three-electrode cell should be used.

While the potentiostat allows determining changes in $\bar{\mu}_e$ of the electrodes, by measuring E_{cell}, nothing has yet been said of $\bar{\mu}_e$ in the electrolyte. While no free electrons exists here, they could still be added through a charge transfer reaction if thermodynamically favourable. An electron electrochemical potential in the electrolyte $\bar{\mu}_e^{el}$ can therefore be defined which will be dependant on the electrochemical potentials of the species involved in the charge transfer reactions [17, 18]. How changes in $\bar{\mu}_e^{el}$ can be probed with APXPS is an essential part of this thesis, and what that can tell about interactions at the interface will be discussed in Chapter 4.

Running the cell as a galvanic cell, the maximum energy that can be output is given by the change in the total Gibbs free-energy

$$\Delta G = -nFE_{cell} \tag{2.12}$$

where n is the number of electrons that are involved in the redox reactions of the cell. Note that this energy is different from the one in equation 2.5, which was denoted the chemical Gibbs free energy, neglecting electric contributions. In order to utilise this energy in a battery, reactions have to take place both at the WE and CE, in order to produce a net current in the external circuit [1, 17]. At the *cathode*, a reduction of the charge carriers in the electrolyte takes place, leaving a neutral species on or in the electrode. Through the external circuit, the electrons will pass the application before oxidising another neutral species on the *anode*. Which one of WE and CE acts like the cathode or anode, will shift as the cell shifts between being a galvanic or electrolytic cell. It is therefore recommended in the battery community to instead denote the electrode of higher electrode voltage (i.e., the lowest electron electrochemical potential) at OCV the *positive electrode* and the other the *negative electrode* [33, 34]. With these conventions established, the interfacial concepts introduced here provide the foundation for understanding the operation and design of lithium-ion batteries, which are the focus of the following chapter.

Chapter 3
Lithium-ion batteries

The success of the lithium-based batteries can be derived directly from the electrochemical potential of the lithium electrode. Lithium has the lowest reduction potential of any stable element, at -3.04 V vs. the standard hydrogen electrode [1, 35]. Pairing it with any other positive electrode material the resulting E_{cell} will therefore be very high, leading to a high energy output as given by Equation 2.12. This therefore leaves lithium-based cells as particularly attractive candidates for storing energy. As seen in Equation 2.4 the electrochemical potential of neutral lithium in a phase α can be expressed by the sum of $\bar{\mu}_e^{\alpha}$ and $\bar{\mu}_{Li^+}^{\alpha}$. A model of the potentials in a lithium-based cell can be seen in Figure 3.1. Striving to minimise the total electrochemical potential the lithium ions will redistribute themselves, as they are the only charge carries able to do so. This will in turn lead to adjustments of $\bar{\mu}_e$ in the two electrodes, creating a cell voltage. Using this model it can be seen that E_{cell} stems from the difference in μ_{Li} between the two electrodes. The shuttling of lithium between electrodes as the battery is operated will change the chemical potentials of the electrodes, and thereby change E_{cell} [36].

3.1 The reactivity of lithium metal

In an idealized case, the most favourable negative electrode would be metallic lithium itself, as it combines the electrochemical potential with the highest possible specific capacity among practical electrode materials. In a lithium metal battery (LMB), energy storage and release take place via the direct plating and stripping of Li at the lithium metal/electrolyte interface. During discharge (i.e battery working as a galvanic cell), lithium metal is oxidized at the negative electrode, releasing electrons to the external circuit while lithium ions gets solvated in the electrolyte and migrate toward the positive electrode, where they are *intercalated* into the positive electrode material. During charging, this process is reversed, and lithium ions are reduced and plated back onto the negative electrode surface. Intercalation denotes the process where the lithium ion is inserted into a host matrix, which lowers the electrochemical potential of the neutral lithium [37, 38].

In practice, however, realising LMBs is severely constrained by the high reactivity of the metallic anode. Upon contact with the electrolyte, the metal surface undergoes spontaneous reactions that lead to the formation of an interfacial passivation layer. This is the *solid electrolyte interphase* (SEI) which is undoubtedly one of the most important parts of lithium-based cells as it prevents further decomposition of the electrolyte while being conductive to lithium ions, enabling the continued movement of lithium across it [2, 39–41]. The importance and implications of the SEI will be discussed in a later section. However, a further consequence of the high reactivity and non-ideal interfacial behaviour of metal electrodes is the tendency for irregular metal deposition during charging. Rather than forming

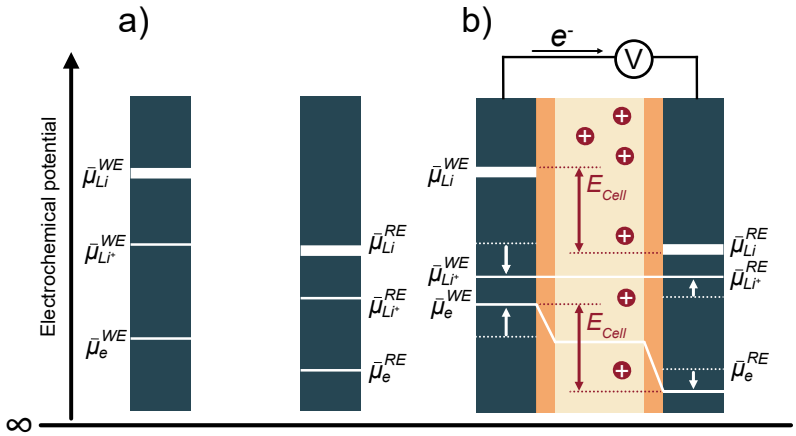

Figure 3.1: Without electrolyte the electrochemical potentials of the metallic lithium, lithium ions and electrons in the two electrodes can be seen schematically in a). All potentials are referred to the vacuum level. When electrolyte is added (b), $\bar{\mu}_{Li^+}$ will strive to equilibrate as it is the only charge carrier able to do so, forcing $\bar{\mu}_e$ to shift. E_{cell} is thereby defined by the difference in the chemical potential of lithium $\bar{\mu}_{Li}$. Figure adapted from [36].

a flat, uniform surface, the metal commonly deposits in a non-uniform manner, creating pointy or porous structures [42]. Over time, this leads to the growth of filament-like structures known as dendrites. Dendritic growth not only accelerates interfacial degradation as new lithium surfaces are exposed but also presents a significant safety risk, as growing metal protrusions can penetrate the separator and cause internal short circuits [37, 43]. Almost all commercial lithium-based batteries today are therefore of a host type where the metallic lithium anode is replaced with an electrode material that can host lithium through intercalation or alloying. This makes the lithium in the negative electrode less reactive and the matrix can shrink and expand as lithium is inserted and removed. As a result, intercalation batteries offer greatly improved cycling stability and safety compared to their metal-based counterparts. This comes at the cost of a reduced energy density due to the increased volume of the negative electrode material [33, 38].

3.2 The intercalating LIB

Sometimes nicknamed the ”rocking-chair-battery” the intercalating LIB was proposed by Armand in the 1970s [44]. The central challenge in the early development of intercalation batteries was to identify host materials capable of reversibly accommodating lithium ions while maintaining structural integrity, favourable electrochemical potentials, and long cycle life. On the negative electrode side, graphite emerged as the preferred intercalation material [37]. Graphite is an ordered carbonaceous material composed of sp^2-hybridized carbon atoms arranged in sheets of hexagonal rings. These sheets are in turn stacked and held together

by weak van der Waals interaction, creating layers for the lithium ions to insert themselves. The weakness of the interlayer bonding facilitates lithium insertion and extraction as the distance between layers can change without to much stress in the material. Electrochemically, graphite exhibits a voltage of 0.1 V vs Li/Li^+, when fully lithiated [33, 38]. This means that E_{cell} is largely retained with relatively small energy losses compared to LMBs. The combination of low operating potential and structural stability has made graphite the benchmark negative electrode material in lithium-ion batteries. Nevertheless, alternative materials have been explored to further increase energy density. Silicon, for example, can alloy with lithium to achieve substantially higher specific capacities, though its large volume changes during cycling, inducing crack in particles and the SEI, pose significant mechanical challenges [45, 46].

On the positive electrode side, lithium-ion batteries typically employ transition metal-based materials that host lithium ions within layered , spinel, or olivine oxide crystal structures. Common cathode materials include lithium cobalt oxide (LCO), lithium nickel manganese cobalt oxides (NMC), and lithium iron phosphate (LFP) [47, 48]. They all differ in redox potential and intercalation mechanism, resulting in batteries with distinct voltage profiles and energy densities [49]. Compared to the other cathode materials, LFP exhibits a very flat cell voltage curve as it undergoes a two-phase transformation as the lithium is inserted [50, 51]. Due to this plateau, LFP been utilised in certain works as a quasi-reference electrode, as small changes in lithium stoichiometry has minimal effect on its electrochemical potential [52–54].

Despite the improved stability offered by intercalation chemistry intercalation electrodes operate at electrode potentials that lie outside the thermodynamic stability window of most organic electrolytes [1]. In addition to the formation of the SEI on graphite [55], a *cathode electrolyte interphase* (CEI), has also been shown to form due to the oxidation of the electrolyte at high voltage cathodes [56–58]. The CEI has been much less studied than the SEI, and it has sometimes been discussed to be of less importance due to the electrolyte decomposition being less prevalent on the positive electrode side [11, 58]. They are also typically thinner and may partially overlap with the decomposition of the cathode material [59, 60]. The SEI is generally more critical to cell stability and will therefore be the primary focus of this work.

3.3 The solid electrolyte interphase

A good passivating SEI should be electronically insulating, preventing continuos electrolyte decomposition, but still allow lithium ions to pass through to the electrode for intercalation. Preferably it should also be chemically and mechanically stable as the battery is charged and discharged to ensure stable cycling of the battery [37]. SEI formation occurs when a solvated lithium ion approaches a sufficiently negatively polarised electrode surface. Due to the strong electrostatic interaction between Li^+ and its surrounding solvent molecules, the ions in the primary solvation sheath are carried toward the interface as a coordinated complex. At the low reduction potentials encountered at the negative electrode,

these solvent molecules are thermodynamically unstable and undergo reductive decomposition. Consequently, the structure of the lithium solvation shell plays a decisive role in determining the chemical pathways available for electrolyte reduction and thus the nature of the SEI that is formed [1].

Commercial and state-of-the-art lithium-ion battery electrolytes typically consist of mixtures of carbonate solvents combined with a lithium salt and functional additives. This reflects the fact that no single solvent fulfils all required properties simultaneously. Cyclic ester carbonates, such as EC, are primarily included to promote the formation of a stable, passivating yet ion-conductive SEI, while linear carbonates, such as diethyl carbonate (DEC) and dimethyl carbonate (DMC), are added to reduce viscosity and enhance ionic conductivity. Additives are further used to fine-tune interfacial stability and electrochemical performance [11, 33]. EC is frequently mentioned as a key solvent for forming a stable and ionically conductive SEI [61, 62]. In contrast, PC, despite its chemical similarity to EC, fails to form a protective SEI on graphite under standard conditions. In PC-based electrolytes, solvent co-intercalation into graphite layers is commonly observed, followed by decomposition due to the low potential of the electrode. The associated gas evolution and volumetric stress are believed to cause exfoliation and mechanical breakdown of the graphite structure. While the precise origin of this stark difference between EC and PC remains unsolved, several hypotheses have been proposed. These include differences in the solubility of decomposition products, with PC-derived species being less likely to precipitate and adhere to the graphite surface, as well as subtle variations in molecular dipole orientation that influence solvation structure and anion coordination [63, 64].

It has been reported that anions are generally less directly involved than solvated lithium ions and solvent molecules, as they are electrostatically repelled from the negatively polarized electrode surface. However, certain anions containing fluorine, such as PF_6^-, FSI^- and $TFSI^-$, have been proposed to undergo chemical or electrochemical decomposition to form neutral or weakly charged species [1, 65, 66]. These decomposition products are assumed to be able to access the IHP, where they further decompose and contribute to the SEI.

Surface-sensitive characterization techniques such as XPS, along with infrared spectroscopy and mass spectrometry, have revealed that the SEI is chemically heterogeneous. Commonly reported inorganic components include lithium oxide (Li_2O), lithium fluoride (LiF) and less common lithium carbonate (Li_2CO_3), while organic constituents such as lithium ethyl carbonate (LEC), lithium ethylene dicarbonate (LEDC), lithium methyl carbonate (LMC) and lithium ethyl methyl carbonate (LEMC) were observed depending on solvents used [67–71]. Structurally, the SEI is often described using either a mosaic or multilayer model, with patches of different chemical components. Imaging techniques, including atomic force microscopy, scanning electrochemical microscopy and cryogenic electron microscopy, suggest that the interphase comprises a dense, inorganic-rich inner layer adjacent to the electrode surface and a more porous, organic-rich outer layer in contact with the electrolyte [68, 72, 73]. The total thickness of the SEI is generally reported to be on the order of a 10-50 nm, although its exact thickness is hard to probe due to its compositional gradients and dynamic nature [11, 74].

3.3.1 The EDL and the SEI

Due to how the EDL changes the position of charged species and governs which electrolyte species are brought into close proximity with the electrode surface, it follows that it plays a decisive role in determining the chemical composition and structure of the SEI [75, 76]. Despite this, the explicit influence of the EDL on SEI formation has received relatively limited attention in battery research until recent years. Some computational studies have addressed this gap by explicitly incorporating EDL effects into interfacial models [29, 77–79].

In one recent molecular dynamics study by Wu et al., the local concentrations of solvent molecules, cations, and anions within the EDL were evaluated as a function of electrode charge for both ether-based and carbonate-based electrolyte systems [80]. By reconstructing the probability distributions of lithium primary solvation sheath structures within the EDL, the authors demonstrated that the solvation environment of lithium differs markedly from that in the bulk electrolyte and is dependent on the charge of the negative electrode. Subsequent density-functional theory calculations revealed that species in these interfacial solvation structures exhibit reduction potentials that deviate from those in the bulk, highlighting the importance of the EDL on the onset of electrolyte decomposition. Interestingly, their model also suggest that, contrary to many experimental studies, anions such as PF_6^- and $TFSI^-$ do not participate in the formation of the SEI in carbonate electrolytes at all. The overall conclusion is that the strength and profile of the EDL can modify the structure of the salvation shells and are therefore needed to predict the reduction mechanisms in the SEI.

Naturally, the creation of an ionically conductive (and electronically non-conductive) phase, such as the SEI, will in turn induce a new potential profile of the EDL and change the environment for further electrolyte reduction and lithium intercalation. Work on this is, however, even scarcer. Previous post-mortem work on cycled graphite electrodes using XPS has shown that an electrochemical potential drop across the buried interface between electrode and SEI exists even after cell disassembly [6, 81]. A model was proposed based on the formation of an electric potential gradient from the accumulation of charged species at the buried interface, for example polar solvent molecules or decomposition species, with another hypothesis being the formation of a capacitive interface between two phases within the buried interface. However, the exact cause of the gradient is not yet clear.

A recent article by Kim et al. highlights the challenges with probing both the potential profile of the EDL, the local concentrations of electrolyte species and the chemical composition of the SEI, and propose combining advanced characterisation techniques as a means of probing both electrostatic and chemical information at the electrode/electrolyte interface [82]. They conclude that SEIs and EDLs should be viewed as indispensable and interrelated interfacial structures and argue that electrode/electrolyte interfaces must be studied "holistically" rather than as isolated components. While no single characterisation technique has been shown to fully resolve this complex interfacial interplay, APXPS provides a valuable starting point as it offers surface sensitivity combined with chemical specificity

and access to electronic state information. The following chapter will therefore introduce XPS and APXPS and discuss its capabilities and limitations in the context of probing battery electrode/electrolyte interfaces.

Chapter 4
Ambient-pressure XPS

There are many techniques for studying batteries, and these can be broadly grouped into different categories. Imaging techniques, such as scanning electron microscopy (SEM), transmission electron microscopy (TEM), and X-ray tomography, are well suited to visualise morphological and structural features, making them useful for observing how structures evolve and form within the battery during operation [42, 83]. Diffraction-based techniques, including X-ray diffraction (XRD) and neutron diffraction, provide complementary information by revealing crystal structure, phase composition, and symmetry of the involved materials [84, 85].

The strength of spectroscopy techniques, such as X-ray photoelectron spectroscopy (XPS), are their sensitivity to not only detect which chemical species are present in a material but also identifying chemical states and quantities of these species. With XPS, while depending on the lateral resolution of the instrument used, it is also possible to determine the spatial distribution of elements on the surface and the thickness of thin overlayers due to its high surface sensitivity [86]. More overlooked within the battery field, however, is the possibility to probe the electrochemical potential of electrons in samples using XPS. There is a close relationship between the Fermi level of an electron and its electrochemical potential in a phase, which, although derived from distinct areas of physical chemistry, are in fact equivalent quantities [17]. Furthermore, while XPS is typically performed under ultra-high vacuum conditions due to the short mean free path of emitted electrons in gases, ambient-pressure XPS (APXPS) overcomes this limitation by enabling measurements at elevated pressures, allowing the introduction of liquids such as electrolytes into the analysis chamber. In this chapter the fundamentals of APXPS will therefore be presented along with the methods used to study battery cells and their interfaces, including synchrotron experiments.

4.1 The photoelectric effect

The underlying phenomenon behind photoelectron spectroscopy is the photoelectric effect, which describes the emission of electrons from a sample when it is exposed to photons of sufficient energy. When a photon is absorbed, its energy is transferred to an electron, and if this energy exceeds the binding energy and the energy needed to bring the electron to the outermost edge of the atom, the electron is emitted, with any excess energy appearing as its kinetic energy (KE). If the photons interacting with the sample have a fixed energy $h\nu$, the KE will only depend on the binding energy BE of the electrons. The BE is most often referenced to the Fermi level E_F of the sample, and the energy needed to bring an electron from this energy level to just outside of the atom is instead expressed by the work function ϕ_{sample}, as can be seen in Figure 4.1a. Additionally, any changes in the chemical potential of the electron will result in a change of the BE

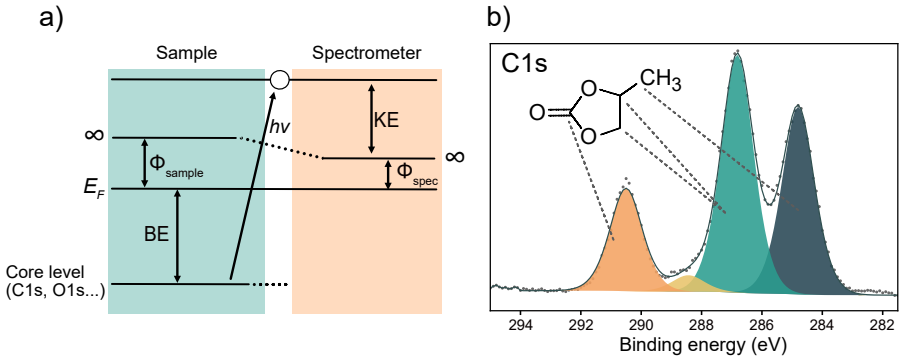

Figure 4.1: a) Diagram over the energy levels involved in the measurement of a photoelectron. After being emitted from a core level, the kinetic energy of the electron will be measured by the spectrometer. The work functions ϕ of the sample and spectrometer is the difference between their respective Fermi levels and the vacuum level ∞. b) An XPS carbon 1s spectrum showing the peaks of the PC molecule. Depending on the surrounding atoms, the core level electrons will experience different binding energies.

with respect to E_F, resulting in a *chemical shift* of the BE and KE [86].

Measuring the KE of the electrons with a spectrometer therefore can give information about the chemical state. However, the measurement of any free electron by the spectrometer must involve adding the electron to the E_F of the spectrometer itself, overcoming the work function of the spectrometer ϕ_{spec}. As a result, the measured KE depends not only on the original BE of the electron but also on the instrumental energy reference. To simplify, the sample is electronically grounded to the spectrometer, thereby aligning their Fermi levels. The measured KE can thereby be expressed through,

$$KE = h\nu - BE - \phi_{spec} \tag{4.1}$$

where ϕ_{spec} will depend on the XPS instrument used. Due to the relation between KE and BE as described in Equation 4.1, XPS data can be plotted with either one as x-axis. However while the KE will depend on the energy of the incoming photons $h\nu$, BE will not [86, 87]. To follow convention, the KE energy scale is depicted as going from left to right while the BE energy scale goes from right to left.

4.1.1 The chemical shift

Both electrons originating from the deeply bound core levels, close to the atomic nucleus, and from the more weakly bound valence bands might be emitted in the photoelectron process. While the valence electrons may by emitted by lower photon energies, and are studied within the area of ultraviolet photoelectron spectroscopy, XPS focuses on core levels. Their BEs are characteristic of specific elements and they do not participate directly in chemical bonding like the valance electrons. The BE of these core levels, however, are highly sensitive to the local

electronic environment and can vary with the charge distribution at the atomic site. Consequently, changes in chemical bonding and oxidation state lead to shifts in core level BE [88, 89]. This can be seen in Figure 4.1b, where the BEs of the emitted electrons coming from the 1s orbital of carbon atoms in a PC molecule are shown. While all electrons contributing to the peaks belong to the same core level, C1s, the peak positions show that the surrounding atoms will affect the BE of the electron. The peak furthest at lowest binding energy of approximately 284.5 eV originates from photoelectrons emitted from the carbon in the CH_3-group. When carbon atoms are bonded to more electronegative elements, such as oxygen, these atoms withdraw electron density from the carbon. This reduced electronic screening increases the effective nuclear charge experienced by the core electrons, resulting in a higher core level BE [86]. Therefore the C–O and especially the CO_3 peak can be seen at the higher BEs of 287 eV and 290.5 eV, respectively.

Chemical shifts arising from changes in local bonding are, however, not the only effects that can lead to peak shifts in XPS spectra. Other contributing factors are spin-orbit coupling, differences in electric charge of the probed species and final-state effects, where the core hole left by the emitted electron induces processes that affect the BE of subsequently emitted electrons [87, 88]. Of particular importance for this thesis is peak shifting caused by changes to the electrochemical potential $\bar{\mu}$ of species within the probed phase. Before discussing this effect in detail, the following section will first describe how the emitted electrons are measured by the spectrometer.

4.2 Measuring photoelectrons

To measure emitted photoelectrons, an XPS experiment requires a sample, an X-ray source, an electron analyser equipped with focusing lens and a detector, all connected to the analysis chamber. These components are typically placed under vacuum conditions for two main reasons. Firstly, a free electron, especially of lower KE, will not travel far in a gaseous environment without interaction with molecules, thereby loosing KE and with it information about the BE in the sample [86, 90]. Therefore analysis chambers requires pressures on the order of $10^{-5} - 10^{-6}$ mbar ($0.1 - 1$ mPa) [88]. Most XPS chambers, however, operates at considerably lower pressures, typically $10^{-8} - 10^{-10}$ mbar. This is because XPS is an extremely surface sensitive technique, and even within seconds at higher pressures gaseous species will adsorb onto the surface of a material, forming a monolayer that can dominate the measured signal rather than the underlying sample [86, 88].

4.2.1 The electron analyser

The electron analyser is responsible for collecting photoelectrons emitted from the sample, spatially separating them depending on their energies. Emitted electrons are first guided toward the analyser by a set of electrostatic focusing lenses, which define the acceptance angle of the electrons and can also filter out electrons from unwanted KE ranges [86]. The most widely used analyser configuration for achieving high energy resolution in XPS is the concentric hemispherical analyser

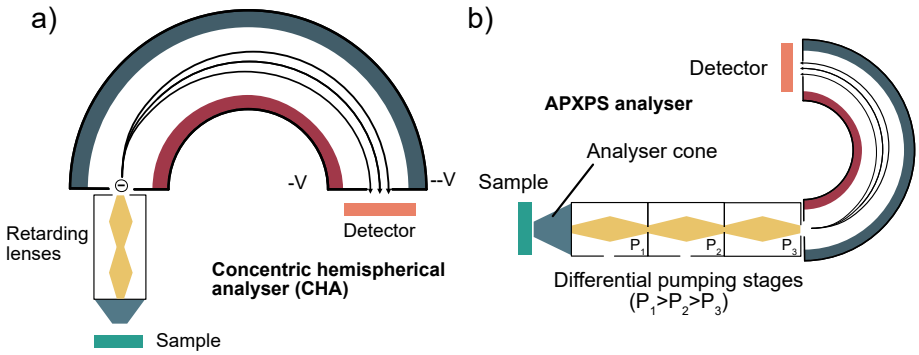

Figure 4.2: a) The CHA is the most commonly used electron analyser due to its high resolution. The retarding lenses will select the wanted electrons and the CHA will spatially disperse the electron on the detector by applying a radial electrostatic field. b) To be able to introduce liquids into the analysis chamber, a differential pumping system must be utilised where the pressure is gradually lowered from (near ambient conditions) around the sample until reaching ultra high vacuum at the entrance of the analyser.

(CHA). As shown schematically in Figure 4.2a, it consists of two concentric hemispherical electrodes held at different voltages. Electrons entering the analyser are spatially dispersed depending on their KE as they travel in the field between the electrodes. Only electrons with a specific KE, determined by the defined *pass energy*, follow a stable trajectory and reach the exit slit, while electrons with higher or lower energies are deflected away. When collecting data for a spectrum the analyser can be operated in two modes: either the voltage is swept by the CHA electrodes, keeping a relative energy resolution across the spectrum, or the electrons are retarded to a fixed pass energy by the lenses before reaching the CHA, resulting in a constant energy resolution [86, 87]. The final energy resolution given by the analyser will therefore depend on the set pass energy, how stable the voltages of the hemisphere electrodes are, the area of the entrance slit and the sensitivity of the detector after the CHA. For newer spectrometers the energy resolution can reach as low as < 10 meV [88, 91, 92].

4.2.2 Enabling liquids in the analysis chamber

The ultra-high vacuum conditions required for conventional XPS make the measurement of liquid samples effectively impossible, as liquids would evaporate almost instantaneously under such low pressures. Consequently, techniques enabling XPS measurements at elevated pressures were developed soon after the introduction of the first XPS instruments [93]. The approach used to achieve this has remained largely unchanged since then. In APXPS, a series of differential pumping stages are positioned between the entrance to the focusing lenses and the entrance of the CHA. At each stage, the pressure is progressively reduced, ultimately reaching ultra high vacuum at the analyser entrance. A schematic representation of this arrangement is shown in Figure 4.2b. This design allows

the same analysers used for regular XPS instruments to be used also for APXPS measurements [93, 94]. A downside of the differential pumping is, however, the reduced electron collection angle, as only small apertures can be used between the pumping stages to maintain the pressure gradient, leading to less electrons reaching the detector. In addition, electrons must have significantly higher KE to traverse the gas phase without excessive scattering, which makes the use of higher photon energies needed. X-ray sources are commonly categorized into soft (<2 keV), tender (2-7.5 keV), and hard (>7.5 keV) X-rays, with tender or higher photon energies typically employed in APXPS experiments [95, 96]. The sample must also be situated closer to the analyser cone to minimise the path of the photoelectrons, with distances decreasing from cm to µm. Depending on the type of atmosphere and system, measurements over a wide range of pressures can be performed. Lab-based systems can operate at pressures up to approximately 100 mbar [97, 98] as claimed by the manufacturers, whereas large-scale facilities, such as synchrotron-based APXPS endstations, which will be discussed below, typically can operate at pressures up to 1 bar [99, 100]. Evaporation of liquids will nevertheless still occur, meaning that measurements of liquid samples within the analysis chamber will also include some signals from the gas phase.

4.2.3 Synchrotron experiments and the HIPPIE beamline

So far, the X-ray source itself has not been discussed. X-rays are typically generated by bombarding a metallic anode with electrons emitted from a heated filament. The choice of anode material determines the characteristic photon energy produced, allowing different energies to be selected. To improve spectral quality, a monochromator is commonly used to reduce the energy spread of the emitted X-rays, as the achievable energy resolution in XPS cannot exceed the line width of the photon source [86]. In practice, it is the X-ray line width, rather than the electron analyser, that sets the lower limit of the energy resolution in lab XPS measurements [87]. One of the key advantages of *synchrotron* radiation is its narrow bandwidth, which enables improved energy resolution. Perhaps even more important benefits are the high photon flux and the tunability of the X-ray energy, providing higher flexibility compared to laboratory sources [101]. A synchrotron is a large circular particle accelerator which utilises magnets to bend the trajectory of electrons travelling close to the speed of light. It consists of an electron accelerator, a booster ring and a storage ring in which electrons circulate in vacuum. The diameter of the larger electron storage ring at the MAXIV synchrotron, located in Lund Sweden, is 528 m [102]. Along the storage ring, multiple beamlines are installed, each of which hosts one or more end-stations where X-ray radiation is delivered and made available for experiments (Figure 4.3a). Just before the end-stations, in straight sections of the ring, either undulators or wigglers are placed, which both consists of series of magnets with alternating polarity. These force the electrons to move back and forth perpendicular to the trajectory in which they move, causing the electrons to emit coherent X-rays with high flux. Controlling the undulator together with a monochromator at the beamlines enables the users to select and change energy to the needs of their experiment.

The experiments of this thesis were performed at the solid-liquid end-station of

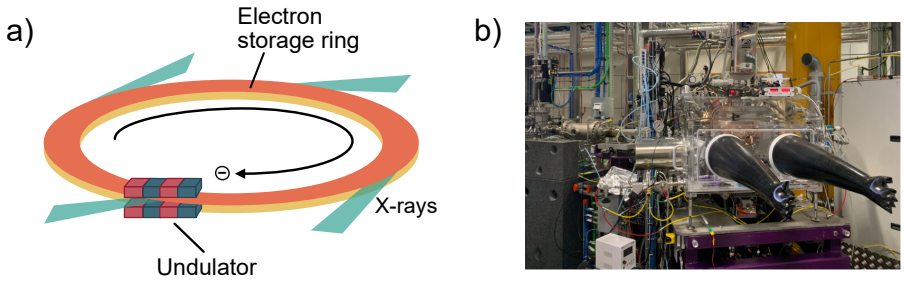

Figure 4.3: a) A very simplified model of a synchrotron. Electrons are travelling close to the speed of light inside the electron storage ring. Groupings of magnets, such as the undulator, move the electrons back and forth causing X-rays to be emitted. The X-rays can thereafter be used at the beamlines and endstations along the ring. b) The solid-liquid endstation at the HIPPIE beamline at MAXIV. In the foreground is the glovebox filled with argon enabling samples to be handled in an inert atmosphere. X-rays enter the chamber from the left in the image through the metal tubes.

the HIPPIE beamline at MAXIV, seen in Figure 4.3b. Its energy range is 0.25 to 2.2 keV, spanning soft and lower region tender X-rays and the analysis chamber is equipped with differential pumping stages that enable APXPS measurements [99]. In addition, a glove box can be attached to the analysis chamber to provide an inert atmosphere for sample mounting. As lithium-based samples are highly sensitive to both oxygen and moisture, maintaining an inert environment is crucial for the experiments presented in this work. The end-station glovebox was filled with argon, and samples could be transported from the laboratory glovebox to the end-station in sealed pouches, ensuring that no exposure to air occurred.

4.3 Combining APXPS and model battery cells

APXPS enables the introduction of liquids into the analysis chamber and has therefore been applied to study electrochemical aqueous systems, where electrolytes were shown to be stable and withstand significant evaporation [96, 103, 104]. In contrast, extending APXPS to battery-relevant electrolytes presents additional challenges, as many commercially used carbonate solvents exhibit vapour pressures that are too high to be sustained under typical APXPS pressures. Common linear carbonates such as DMC and DEC readily evaporate, rendering them unsuitable for stable measurements [105]. EC has a sufficiently low vapour pressure but is solid at room temperature, which complicates its use in experiments where the temperature can not be raised. As a result, PC emerged as the first battery-relevant electrolyte solvent to be successfully investigated using APXPS at an analysis chamber pressure of around 0.2 mbar [105]. Under optimised conditions using PC vapour as the background gas, evaporation of PC-based electrolytes was found to be sufficiently slow to allow acquisition of well-defined spectra (up to 1 h).

4.3.1 Dip-and-pull experiments

Another remaining challenge of measuring electrode/electrolyte interfaces with APXPS is the horizontal orientation of the electron analyser, which complicates probing liquid surfaces. This geometry is dictated by the standard analyser design and beamline layout at synchrotron facilities and is therefore fixed. This geometry, however, can also be advantageous as it facilitates the formation of thin electrolyte films that can be probed simultaneously with the electrode. Axnanda et al. therefore proposed the first dip-and-pull measurement where a flat electrode is dipped and subsequently pulled from the electrolyte so that a thin meniscus forms on the surface [95], as shown in Figure 4.4a. In this configuration, electrodes are mounted vertically on an a specialised sample holder connected to a manipulator that can be moved in three directions. The WE, RE and CEs are mounted in a stacked geometry so that the WE, which is the electrode of interest for the APXPS measurements is facing the analyser. A picture of the real electrode setup in the analysis chamber is shown in Figure 4.4b. The electrodes are connected by electrical contacts in the sample holder to a potentiostat outside of the analysis chamber and the WE is electrically grounded to the spectrometer, aligning their Fermi levels. The electrodes are thereafter dipped into a beaker with electrolytes so that a meniscus forms. Therefore, a voltage or current can be applied between the electrodes while the liquid meniscus on the WE can be measured with APXPS.

The thickness of the meniscus formed will depend on the surface tension of the electrolyte and electrode material, concentration and pulling speed of the sample holder, but for PC-based electrolytes on a flat and non-porous electrode is approximated by eye to be the µm range after the electrodes are freshly dipped. The photoelectron inelastic mean free path in PC can be approximated using the TPP-2M formula, and is ∼5 nm for an electron with a kinetic energy of 1500 eV [106], giving an approximate probing depth of 15 nm, if typical photon energies around 2 keV are used. If this value is smaller than the meniscus thickness, both the electrode and electrolyte could be probed simultaneously. This has been done in several works using aqueous electrolytes where the meniscus typically is thinner than for PC-based electrolytes. These works have given much insight into the reactions, potentials and energy levels at the interface over a wide range of research topics, such as semiconductor junctions [96], catalysis [104, 107, 108] and corrosion [109, 110] to name some. A recent work claims that SEI formed on a glassy carbon (GC) electrode in PC electrolyte can be probed through a 1 nm thin precursor film at the top of the meniscus, that precedes the meniscus layer [111]. Later work from Krizan et al., also using PC electrolytes, demonstrated however, that much thicker menisci than this (∼20 nm) exhibited two to three orders higher resistance than the bulk electrolyte [112]. It therefore remains uncertain whether such a thin precursor layer can sustain electrochemical reactions comparable to those occurring in the bulk electrolyte.

4.3.2 Probing the thick meniscus

An alternative measuring approach is to not measure the electrode/electrolyte interface directly but instead only probe the thicker part of the meniscus, where no

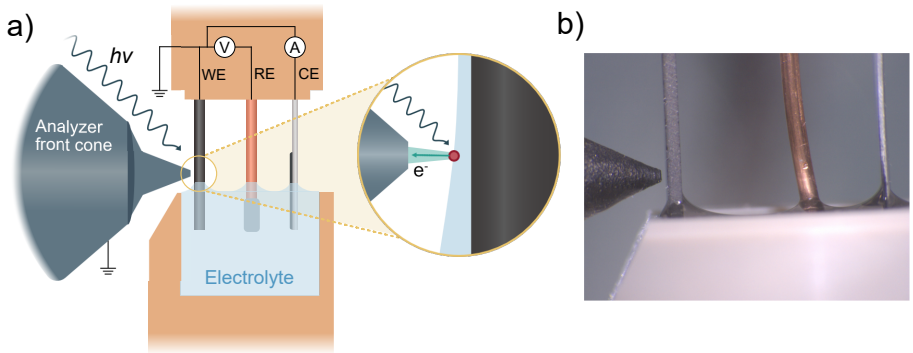

Figure 4.4: a) The measurement setup for a dip-and-pull cell measured by APXPS. The electrodes are attached on a specialised sample holder that can be dipped and pulled out of the beaker of electrolyte. The WE is grounded to the spectrometer. b) A close up of the three electrodes dipped in the electrolyte. Due to the elevated pressures, the analyser cone must be kept very close to the WE and meniscus.

signal from the underlying electrode is measured. This in case of the meniscus being too thick or the excitation energy too low. Works by Källquist et al., introduced this approach together with an electrochemical model and showed that information about the EDL and changes in chemical and electrostatic potentials could still be obtained about both the electrode and electrolyte [8, 9]. By definition, the Fermi level of a phase is equivalent to the electrochemical potential of the electrons in that phase [12, 17]. Therefore, assuming that the core levels, which can be measured by APXPS, shift together with the Fermi level of the probed phase, changes in Fermi level can be directly correlated to changes in the electron electrochemical potential of the phase $\Delta\bar{\mu}_e^{\alpha}$. This assumption will hold as long as there is no chemical shifts of the BE. Since the WE is grounded to the spectrometer, all spectra taken will be referenced to $\bar{\mu}_e^{WE}$. This makes it possible to probe changes in the electrochemical potential gradient between the electrolyte in the thick meniscus and the WE by measuring any electrons emitted from the core levels of the electrolyte and their peak shifts $\Delta KE = \Delta\bar{\mu}_e^{el} - \Delta\bar{\mu}_e^{WE}$. The electrochemical potential of the WE can be changed by applying a voltage using a potentiostat, as discussed in the previous chapter. If this change and possible resulting charge transfer reactions do not change the chemical potential μ_e^{WE} of the WE, $\Delta\bar{\mu}_e^{el}$ is simply given by the electrostatic contribution $\Delta\phi^{WE}$, which is equal to the change in voltage ΔV. If the chemical potential of electron in the electrolyte is also constant through the process of applying the voltage, the KE shift of the electrolyte peaks can be expressed through $\Delta KE = -\Delta\phi^{el} - (-\Delta\phi^{WE}) = \Delta\phi^{WE} - \Delta\phi^{el}$ with the change in sign coming from $z = -1$ for the negatively charged electron [8, 9]. In the EDL there will be an electrostatic potential gradient affecting all charged species. However, if the measured photoelectrons are originating from electrolyte layers far outside the diffusive layer, the electrostatic field should stay fairly constant, even as the applied voltage is raised [96]. This would then lead to $\Delta\phi^{el} = 0$ for these electrons and $\Delta KE = \Delta\phi^{WE} = \Delta V$. If these assumptions are fulfilled,

changing the voltage between the WE and RE with 1 V would therefore result in the electrolyte peaks in the spectrum shifting with 1 eV.

Measuring changes in peaks originating from the thick meniscus while the cell is under electrochemical bias can therefore provide valuable insight into the electrochemical potentials at the electrode/electrolyte interface. In particular, deviations from the expected 1 eV/V trend could potentially give deeper information about reactions and charge distributions at the surface. Potential origins for deviations from the 1 eV/V trend were summarised by Rotannelli et al. in a recent paper [94]. These are not solely connected to the electrochemistry of the interface but could also be a result of poor meniscus stability. Deviations could stem from (i) changes in the electron chemical potential at the interface induced by Faradaic processes that would lead to the assumption of $\Delta\mu_e^{el}$ and $\Delta\mu_e^{WE}$ not being zero, (ii) the EDL extending beyond the thickness of the film, leading to $\Delta\phi^{el}$ also not being zero, and (iii) instability of the RE resulting in ΔV not being what is expected. Meniscus related issues leading to deviation include (iv) iR-drops due to bad mass transport in the meniscus, causing a drop in the effective ΔV in the meniscus, and (v) complete disconnection of the probed electrolyte on the WE from the bulk electrolyte. Naturally, there could also be more unexplored mechanisms contributing to a deviation. Interestingly, the formation of an SEI has been shown to not lead to a deviation of the 1 eV/V trend when probing the thick electrolyte film [8, 111]. This was motivated by the SEI only forming a passivating surface layer and not changing the chemical potential of the WE. Furthermore any changes to the EDL because of the layer did not cause any changes in the electrostatic potential in the thick meniscus, although it can not be ruled out that the profile of the potential has changed [8]. Just studying the KE response to applied voltage steps does therefore not allow SEI formation to be detected.

While (i) and (ii) could potentially bring more insight into the processes at the electrode/electrolyte interface, deviations stemming from (iii), (iv) and (v) are typically unwanted as they are a product of the cell measurement setup. This is a limitation since the goal of any model system is to be as representative of the real system as possible. In the two papers of this thesis, approaches to distinguish between the mechanisms leading to deviation from the expected trend are therefore presented and evaluated for a model battery system.

Chapter 5
Measuring a model battery system with APXPS

The aim of this work is to develop and apply APXPS measurement approaches that enable improved insight into reactions, kinetics, and electrochemical potentials at LIB electrode/electrolyte interfaces. In particular, the focus is on probing interfacial phenomena, such as SEI formation, under conditions that are closer to real battery operations than *ex situ* measurements where no electrolytes are present. To achieve this, the dip-and-pull technique is used and the comparatively thick part of the meniscus is targeted to attempt to avoid higher resistances in the meniscus compared to the bulk [112].

Not all battery electrode materials are compatible with a dip-and-pull configuration. Commercial battery electrodes typically consist of thin coatings of active material deposited on metal current collectors and are stacked to maximize surface area and energy density. Such electrodes are mechanically fragile and cannot easily be dipped into an electrolyte while maintaining their structural integrity without additional support. Moreover, practical battery electrodes are highly porous, designed to absorb electrolyte and provide ionic access to internal surfaces. For porous electrodes, this prevents the formation of a well-defined and uniform external meniscus in APXPS measurements. As a result, either solid electrodes or very compact, low-porosity model electrodes must be used in this experimental approach.

The model system employed in this work is therefore necessarily simplified. The degree of simplification or alteration of the model system compared to real-life systems depends on the specific measurement objectives, such as whether bulk or surface properties are of interest. In this work, the primary goal is to study surface-limited processes at the electrode/electrolyte interface, including SEI formation and its impact on the electrochemical potentials of species close to the interface. Consequently, it is more important that the surface chemistry and electrochemical behaviour of the WE resemble those of negative electrodes, such as graphite, rather than reproducing a full bulk electrode functionality. Finally, it should be noted that the electrolyte volume used in the beaker-cell setup in dip-and-pull measurements is orders of magnitude larger than that used in commercial battery cells, where typically tens of micro litres are present in standard CR2032 coin/button cells. The beaker used in the experiments of this thesis contained $\sim$8 mL of electrolyte. This must therefore be taken into account when drawing parallels to real-life battery systems in the analysis of the data, particularly with regard to mass-transport processes and electrolyte equilibration.

5.1 A model battery cell

Glassy carbon (GC) was selected as the WE material as it is single phase carbonaceous material and well established electrode material in electrochemistry

[113, 114], making it a suitable model system for graphite electrode/electrolyte interfaces. The electrochemical potential of glassy carbon versus lithium corresponds closely to that of graphite electrodes, with an open-circuit voltage of approximately 3 V vs. Li/Li^+. The smooth and non-porous nature of glassy carbon, however, makes it suitable for dip-and-pull measurements. GC electrodes were previously used by Capone et al. as a negative electrode to study the formation of SEI [111]. In addition, it has been shown that GC forms a SEI of similar chemical composition to that formed on graphite [115, 116]. While on a much smaller scale compared to graphite, GC has also been shown to support intercalation of Li^+ of the surface layers [117]. These factors make GC a suitable negative electrode for model battery systems. Bars of solid GC (50.0x8.0x1.0 mm, HTW, Sigradur G) were polished using alumina slurry and lapping film with a grain size down to 0.3 µm. They were thereafter rinsed in water, sonicated in isopropanol and dried in a vacuum oven at 110°C for at least 12 hours.

As the meniscus of the CE is not measured in this experiment, lithium iron phosphate (LFP) CE electrodes were prepared similar to electrodes for lab-based coin cell testing by mixing LFP (Gelon Energy Corp.), carbon black (Alfa Aesar) and polyvinylidene difluoride (PVDF) (MTI Corp.) in a weight ratio of 80/10/10. The powders were mixed into a slurry by adding the solvent N-metyl-2-pyrrolidon (Supelco) and coated with a doctor blade on 1.0 mm thick aluminium bars. The electrodes were allowed to dry in air for 12 hours and then dried in a Büchi oven in an argon filled glovebox (O_2 <1 ppm, H_2O <0.01 ppm) at 110°C for at least 12 hours. Lithium metal (Toyota Tsusho Corp.) was used as RE. Strips of lithium were cut from an approximately 0.2 mm thick lithium ribbon, rolled and crimped around a 1.3 mm thick copper wire. Just before assembly in the electrode holder the surface of the lithium was scraped to reveal a fresh metal surface.

Two types of electrolytes were prepared to investigate whether the choice of lithium salt would influence the electrochemical processes. In addition, electrolytes with concentrations of both 1.0 M and 0.5 M were used to evaluate possible effects related to mass transport and meniscus drying. Both commercial and self-mixed electrolytes were included. While not universally the case, commercial electrolytes can be expected to exhibit higher reproducibility and potentially lower impurity levels and better compositional homogeneity. Two lithium salts were used: lithium bis(trifluoromethanesulfonyl)imide (LiTFSI) and lithium hexafluorophosphate ($LiPF_6$), both dissolved in PC. Commercial electrolytes (Solvionic) with a concentration of 1.0 M for each salt were used as received and were newly purchased prior to the experiments. Self-mixed LiTFSI electrolytes were prepared in an argon-filled glovebox by dissolving LiTFSI (Solvionic) in battery-grade PC (Sigma-Aldrich) to concentrations of 1.0 M and 0.5 M. Before preparation, the LiTFSI salt was dried at 75°C for 12 hours in a Büchi oven. The solvent was used as received without additional drying. All electrolytes were degassed prior to transfer to the HIPPIE end station by placing them in a Büchi oven under reduced pressure. This step was performed to minimise gas evolution and excessive bubbling during the APXPS measurements.

5.2 Measurement protocols

In the papers of this thesis, different cycling protocols and measurement strategies have been developed to study the evolution of the electrochemical potentials at the electrode/electrolyte interface. Here these APXPS measurement protocols are presented together with a motivation for their use, providing the context necessary for interpreting the results presented in the following chapter.

5.2.1 Studying charge transfer through cell voltage relaxation

So far, formation of the SEI has not yet been able to be distinguished by APXPS using the dip-and-pull technique. In Paper I of this thesis, we therefore propose a new strategy involving open circuit steps during electrochemical cycling. EDLs formed at the WE/electrolyte interface by applied voltages results in an electrochemical potential drop across the interface that can be probed by APXPS. If the external connections between WE and CE are opened and no charge transfer reactions occur, the EDL is expected to remain largely unchanged. Since the surface of the WE is still charged, measuring the electrolyte peak positions should still yield a 1 eV/V relation. If, however, interfacial charge transfer reactions are present, stored charge in the EDL is consumed, leading to self-discharge and relaxation of the electrochemical potential. This relaxation of electrochemical potential between the WE and electrolyte can be measured by APXPS and therefore may provide insight into kinetics ad the interface. The cycling protocol of the relaxation measurements comprised three sequential steps, repeated throughout the experiment and shown in Figure 5.1: (i) a voltage sweep, where the WE potential was linearly driven to a set voltage at a rate of 1 V/s; (ii) a voltage hold, maintaining the WE at the set voltage with respect to the RE by, if needed, adjusting the current between WE and CE; and (iii), the cell was in an open-circuit condition and only the electrode potential was measured to see if relaxation occurs. The dip-and-pull cells were stepped from (ii) to (iii) when the current had stabilised and from (iii) to (i) when the WE relaxation voltage had started to flatten out, both after about 20 and 15 min, respectively.

5.2.2 APXPS measurement settings

The solid-liquid end station at HIPPIE is equipped with a Specs Phoibos-NAP spectrometer, and for all APXPS measurements, a photon energy of 1800 eV was used. The analyser cone of a diameter of 0.3 mm was oriented perpendicular to the GC electrode and at an approximate distance of 0.6 mm, equivalent to two cone diameters. The exact cone to sample distance was determined for each cell individually based on optimal count rate and the spot size of the X-ray beam set to 20×10 µm (V×H). During the measurement, two types of APXPS measurement modes were used, *scanning* mode and *snapshot* mode. The scanning mode allowed for detailed scans of the type shown in 4.1b. For these spectra an energy step size of 0.1 eV and pass energy of 100 eV was used, with each core level measurement spanning 20 eV taking 17 s. These were taken after approximately 15 min of constant voltage (ii) where the current had stabilised, and after 15 min of relaxation (iii).

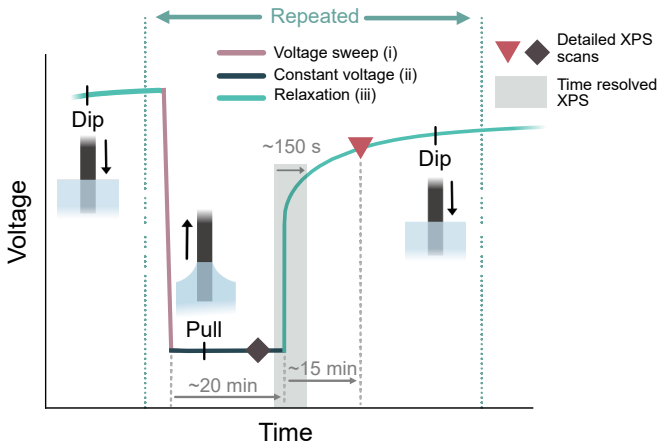

Figure 5.1: The cycling procedure of the relaxation measurement consists of a constant voltage step (i), a voltage sweep (ii) and an open circuit step where the cell voltage is allowed to relax (iii). These steps are repeated at successively lower voltages. During the voltage sweep, the electrodes are dipped in the electrolyte. During the relaxation they are pulled up, allowing for time-resolved measurements to be taken of the meniscus. Additionally, detailed scans are taken both at constant voltage and 15 min of relaxation.

Due to the length of the detailed scans, they can not resolve processes happening on shorter second time-scales. In the snapshot mode, the spectrometer energy window is fixed and spectra are acquired with short acquisition time but high temporal resolution. This results in lower counts per second, and noisier data, but allows for a time-resolved APXPS on sub-second timescales. In the experiments of this thesis, a snapshot (spectrum) was taken every 0.3 s, including dead time between scans. The energy step was set to 0.013 eV and the pass energy 100 eV. During the measurement, the electrodes were constantly moved perpendicular to the analyser cone at a speed of 0.005 mm/s to ensure a fresh spot on the meniscus was probed. The time-resolved measurements were started with the cell in step (ii). After roughly 50 spectra had been acquired, the cell was transitioned to step (iii) and the acquisition continued until 500 spectra had been measured, with the entire time-resolved measurement taking approximately 150 s.

5.2.3 *In situ* vs. *operando* dip-and-pull measurements

For time-resolved measurements, the electrodes must be withdrawn from the bulk electrolyte as the voltage is applied or released. If the electrodes are withdrawn from the electrolyte bath during both applying the voltage and transitioning to OCV, this implies longer exposure of the electrolyte meniscus, which may affect meniscus stability. In Paper II, we therefore investigate the effect of two different measurement protocols that we call *operando* and *in situ*. These two protocols are presented schematically in Figure 5.2 a and b, respectively. In the operando protocol, the electrodes are dipped in the electrolyte once every

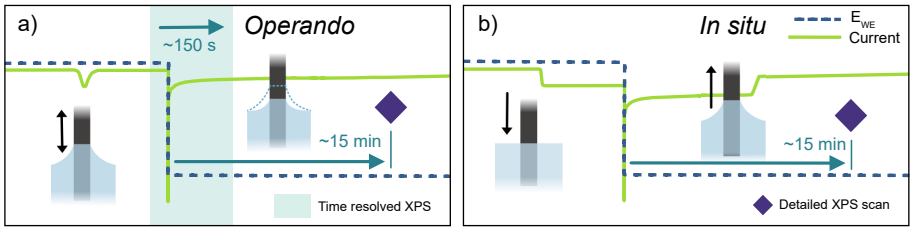

Figure 5.2: a) In the *operando* protocol, the electrodes are only dipped in between cycling steps to reform the meniscus. The voltage step is performed with the electrodes pulled up and the meniscus formed. This allows for time-resolved measurements to be taken at any step in the cycling process. b) In the *in situ* protocol, the voltage is applied with the electrodes dipped in the electrolyte bath. The electrodes are pulled up and the meniscus is formed just before APXPS measurements are taken. Generally, small changes in the current are observed when the cells are either dipped or pulled out of the electrolyte due to slight changes in the electrochemically active area as schematically represented by the green lines.

repeated measurement step. Thereafter, all voltage control and subsequent APXPS measurements are performed with the electrodes pulled up from the electrolyte bath. Between the repeated steps, the electrodes are dipped again, forming a fresh meniscus. This configuration allows time-resolved measurements to be taken during the applied or released voltage. In contrast, for the in situ protocol the electrodes remain immersed in in the electrolyte during this process and are only withdrawn when the cell has reached a steady state (constant voltage or constant current). The differences are therefore the duration for which the electrodes are pulled and the position of the electrodes as the voltage is applied or released. We performed detailed scans 15 min after the voltage set to study possible differences between the described protocols. Paper II assess these differences, identify situations where one may be preferred, and evaluate how protocol choice impacts the reliability of the obtained results.

Chapter 6
Results and discussion

This chapter presents a summary of the main findings of the two papers in this thesis. Paper I shows the results of dip-and-pull APXPS experiments where voltage relaxation is measured to follow the evolution of the electrochemical potential. Paper II discusses differences between the in situ and operando protocols and gives examples of best practices when performing dip-and-pull measurements on model battery systems.

6.1 Studying relaxation behaviour in open-circuit conditions

In Paper I, a number of dip-and-pull cells were cycled according to the voltage relaxation approach presented in Chapter 5. Both detailed scans and time-resolved measurements were taken of the thick part of the electrolyte meniscus before and after the cell was transitioned to open-circuit to investigate interfacial processes at the WE/electrolyte interface.

6.1.1 Peak position vs. cell voltage

Using the C-O peak position from PC for two cells, one with self-mixed 1.0 M LiTFSI in PC and another with commercial 1.0 M LiTFSI in PC, we can follow their shifts with respect to the applied cell voltage, as shown in Figure 6.1. Detailed scans were taken both at constant voltage and after 15 min in relaxation at open-circuit. The relaxation data points are plotted at the voltage from which the cell was released, rather than the actual cell voltage at the moment of the XPS measurement, to more clearly illustrate the correlation with the constant voltage measurement. Figure 6.1a shows the cells as they were cycled down from OCV to 0.3 V and Figure 6.1b shows the commercial electrolyte cell as it was cycled back up to 2.5 V.

While the constant voltage data for all cells looks linear up until approximately 0.5 V, there are some deviations from the expected 1 eV/V trend. Between OCV and 0.7 V, the slopes are 0.90 eV/V for the commercial electrolyte and 0.86 eV/V for the self-mixed electrolyte. In contrast, between 1.5 V and 0.7 V, the extracted slopes are 0.98 eV/V and 1.04 eV/V for the two electrolytes, values that closely match 1 eV/V. After 0.5 V, the deviation from the trend is expected as this represents a voltage region where lithium intercalation in the GC can occur [117]. Here the chemical potential of the electrode is expected to change, reducing the change in ΔKE. Before 0.5 V, lithiation of the GC is however expected to be minimal. As discussed in Chapter 4 on APXPS, a deviation may also be caused by iR-drops in the meniscus which would reduce the effective applied field. This drop is however expected to increase with current which in Paper I was shown to increase with every voltage step. Since the deviation is the largest at higher voltages (where the current is the lowest), this does not explain the deviation.

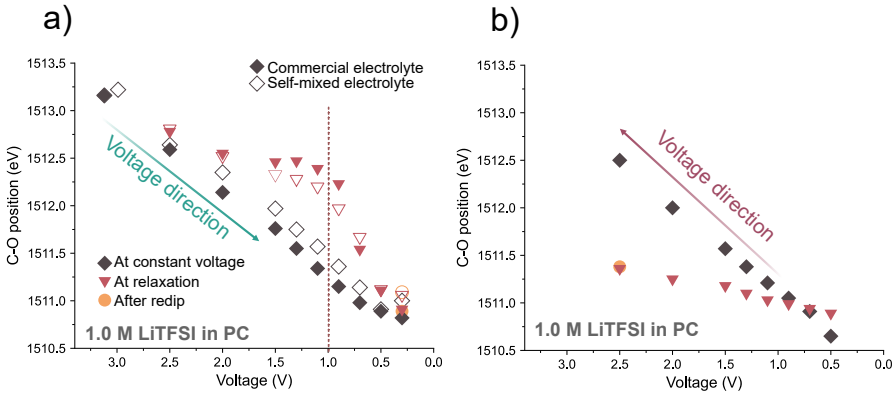

Figure 6.1: a) The kinetic energy position of the C-O peaks as a function of constant applied voltage for commercial (closed symbols) and self-mixed (open symbols) electrolytes as the cell is cycled to progressively lower voltages. b) The return cycling of the commercial electrolyte cell. The relaxation data points (triangles) are plotted at the voltage from which the cell was released, rather than the voltage the time of the XPS scan. The dotted line at 1 V indicates the approximate onset of SEI formation.

Studying the relaxation data points in Figure 6.1a, they show different behaviour to the constant voltage data points. First at higher voltages, relaxation peak positions closely match those obtained during constant voltage holds, but as the voltage decreases they deviate and form a plateau at around 1512.5 eV KE for cell voltages between roughly 2 and 1 V. This indicates that a self-discharge of the electric double layer is taking place, reducing the electrochemical potential difference between the electrolyte and WE. Below about 1 V, the peaks shift again toward the constant voltage values.

PC-based electrolytes containing lithium salts are known to undergo cathodic decomposition between 0.6 and 1 V [118–120]. In Paper I, a similar decomposition voltage was observed for the electrolytes in cyclic voltammograms recorded in a beaker cell in an argon-filled glovebox. Furthermore, the current for the APXPS cell was also shown to increase in this voltage range. The change in relaxation behaviour below 1 V could therefore be attributed to SEI formation, or some related process. Studying the data points of the return cycling up to 2.5 V for the commercial cell (Figure 6.1b), the constant voltage data points follow a very linear trend, however now with a slightly lower slope of 0.9 eV/V. Contrarily, the relaxation data points now follow a linear trend with a slope of 0.24 eV/V across the whole voltage range. At this stage of cycling, lithiation at low potentials has shifted the chemical potential of the WE, resulting in a lower open-circuit voltage, which also results in the relaxation data points being at lower values, as the discharging of the EDL tends towards this new voltage.

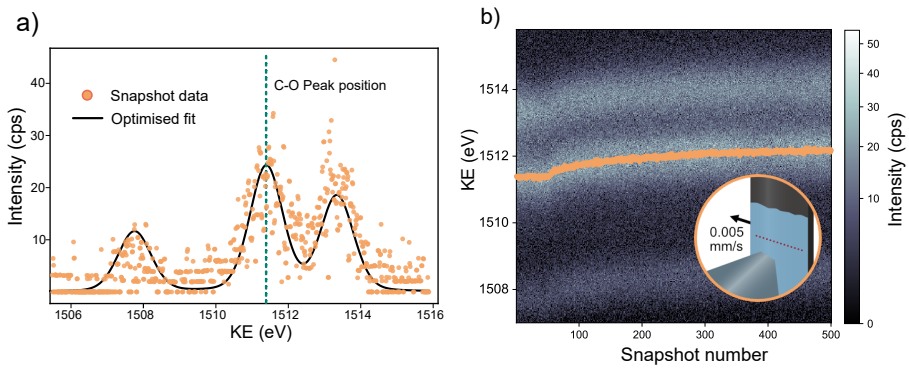

Figure 6.2: a) Each individual snapshot was fitted with an optimisation algorithm. Due to the low acquisition time, the snapshot data is much noisier than for the detailed scans. b) A 2D plot of a time-resolved measurement where the commercial 1.0 M electrolyte cell was released from 1.1 V. The electrodes were constantly moved horizontally during the measurement to avoid beam damage as indicated in the figure inset. The position of the C-O peaks are marked by orange dots. The shifting of dots at snapshot 50 corresponds to the transition from constant voltage to OCV.

6.1.2 Time-resolved measurements

The reason for all deviations from the 1 eV/V trend is however not completely understood, for example the plateau between approximately 2 and 1 V for the relaxation data points, where a slope of around 0.9 eV/V was seen for both cells. In order to study the voltage relaxation process more closely, time-resolved measurements were performed of a cell using commercial 1.0 M LiTFSI in PC electrolyte as the cell was allowed to relax from the constant voltage steps. Figure 6.2a shows a XPS snapshot spectrum together with the optimised fit. This data is much noisier than the detailed scans due to the low acquisition time of less than 0.3 s. A time-resolved measurement, consisting of 500 snapshots, taken as the cell was allowed to relax from 1.1 V is shown in Figure 6.2b. Despite the noisy snapshot spectrum a clear shift of the electrolyte peaks can be seen with the fitted C-O peak positions marked. An advantage of time-resolved measurements is the ability to analyse relaxation profiles and directly compare them with electrochemical data, such as the voltage of the WE, E_{WE}. This enables identifying processes specific to the WE/electrolyte interface as the KE data only will measure difference in electrochemical potential across the meniscus. Moreover, the shape of the relaxation curves can provide additional insight into the nature of the underlying processes. While adopting a 1eV:V scale of the KE axis and E_{WE} is intuitive, aligning the absolute values is less so. Figure 6.3 show two different alignments in a) and b) with the former aligning the two axis at the constant voltage. Due to the higher noise level in the peak positions (Figure 6.3a), they were fitted with a stretched exponential function for clarity. When plotting all time-resolved measurement together, like in Figure 6.3b, only the first constant voltage step at 2.5 V has been aligned with the corresponding initial peak positions. This

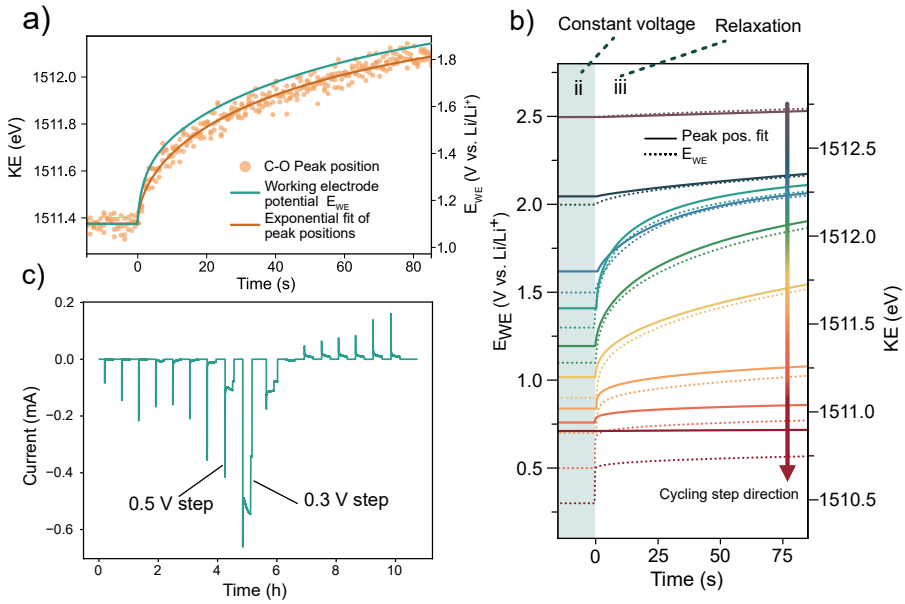

Figure 6.3: a) The position of the fitted C-O peaks, and a stretched exponential function fit of the peak positions are plotted together with the corresponding voltage of the WE, E_{WE} as the commercial electrolyte cell was released from 1.1 V. b) The cell current between WE and CE during the experiment. c) The exponential fit of the C-O peaks as the cell is stepped from constant voltage (i) to relaxation (ii) (solid lines). The corresponding E_{WE} is plotted in the same colour (dotted lines). The two axis have been aligned at 2.5 V and are scaled 1 eV:1 V.

way, also deviations from the 1 eV/V trend become apparent in the figure as a difference between the KE positions (solid line) and the EWE (dotted lines) in the constant voltage set (grey shaded area in Figure 6.3b).

During the initial cycling step from the open-circuit voltage at approximately 3.0 V down to 2.5 V, only minimal relaxation is observed in both the KE peak positions and E_{WE}, indicating that the charge stored in the EDL remains largely unchanged. As the voltage is further reduced from 2.0 V to about 1.1 V, both curves exhibit clear relaxation toward higher KE and higher voltages. In this voltage range, significant SEI formation is not expected, suggesting that the observed relaxation originates from EDL self-discharge rather than surface passivation processes. The observed behaviour here is similar to what is discussed in literature on the self-discharge behaviour of double layer capacitors [121–123]. Charge redistribution on the electrode surface may be a reason for self-discharge but is expected to play a minor role here, as the glassy carbon WE is essentially without open porosities [124]. We instead believe parasitic reactions involving minority species, such as impurities, to be the more likely cause. Possible contributors to the reactions include water reduction, reduction of solvent precursor such as 1,2-propanediol, or reactions associated with trace HF formation from electrolyte

hydrolysis. These reactions would progressively discharge the EDL but slow in rate as the electrostatic driving force decreases, consistent with the observed flattening of the relaxation curves toward approximately 2 V. The shape of the curves would also depend on the diffusion of these species and how quickly they can move to the electrode surface to react.

Below 1 V, the relaxation behaviour changes noticeably. Both KE and E_{WE} curves show a more abrupt initial response and faster stabilization, indicating that different interfacial processes are taking place. This voltage range coincides with typical SEI formation potentials, suggesting that electrolyte decomposition and surface passivation dominate EDL discharge. After initial formation, the passivating SEI would effectively prevent the previous parasitic reactions, no longer causing a slow self-discharge. Below 0.7 V, deviations between KE and E_{WE} increase, consistent with lithium intercalation into GC, which alters the chemical potential of the WE and leads to deviations from the expected 1 eV/V trend. At 0.3 V, no clear self-discharge is observed in the KE peak positions because lithiation has shifted the WE chemical potential, establishing a new OCV close to the applied voltage. As a result, the driving force for further discharge is low. The step observed in the E_{WE} curve, but not in the KE data, is attributed to an iR-drop across the cell, consistent with the increased current associated with lithium intercalation in this voltage range. This can be seen in the current data for the cell (Figure 6.3c), where the current increases significantly during the 0.5 and 0.3 V voltage steps.

6.1.3 Deviations from 1 eV/V due to minority species.

With improved insight into what causes the relaxation behaviour in the model battery system, the remaining unexplained deviations from 1 eV/V can be revisited. In previous works, the high Li^+ concentration in the electrolyte (1.0 M) has been deemed sufficient to maintain a constant chemical potential of both $\mu^{el}_{Li^+}$ and μ^{el}_e in the meniscus during cycling [8, 9]. While no free electrons exist in the electrolyte, the electrochemical potential of an electron in the electrolyte can be defined by the species involved in adding the electron to the electrolyte through redox reactions [18]. In previous works, the relation $\mu^{\alpha}_{Li} = \bar{\mu}^{\alpha}_{Li^+} + \bar{\mu}^{\alpha}_e$ has therefore been used to motivate that if $\mu^{el}_{Li^+}$ stays constant, so does μ^{el}_e [9]. However, this assumption holds only if lithium is the sole redox-active species. Analysis of the time-resolved relaxation data between 2.0 and 1.1 V shows EDL self-discharge, and since this is above the expected onset for SEI, other processes needs to be considered. This includes faradaic reactions with low-concentration impurities such as water and 1,2-propanediol. In this same voltage range, deviations from the ideal 1 eV/V scaling between electrolyte peak position and EWE are observed. The consumption of low-concentration species, during parasitic reactions could potentially generate local concentration gradients near the WE and within the meniscus, violating the constant chemical potential assumption. As a result, the electrochemical potential of electrons in the electrolyte would change locally, leading to a deviation from 1 eV/V. This interpretation remains a hypothesis, and further experiments are required to directly probe the concentration of minority species and assess whether concentration gradients can develop on the relevant

timescales.

6.2 Comparison of in situ and operando protocols

Chapter 4 discussed several possible sources of deviations from the ideal 1 eV/V trend, some of which may arise from meniscus shape and stability rather than stemming from electrochemical effects at the interface. In Paper I, it was shown that time-resolved measurements provide deeper insight into interfacial mechanisms compared to KE vs. applied voltage plots alone. Time-resolved measurements have also been used to investigate iR-drops by correlating delays in KE shifts with electrochemical currents [112]. These measurements, however, require withdrawing the meniscus from the bulk electrolyte for longer periods of time, which could compromise its stability. In Paper II, these aspects were therefore examined by comparing the in situ protocol and the operando protocol to identify strengths, limitations, and reliability of each approach.

6.2.1 Meniscus stability in APXPS measurements

The detailed spectra acquired during constant voltage holds can be directly compared between the in situ and operando protocols. In Paper I, where the in situ protocol was used during the applied voltage step, the cells showed high reproducibility across both self-mixed and commercial electrolytes, as well as for different lithium salts. Figure 6.4a shows the shift of the C-O peak position as the applied voltage between the WE and RE is stepwise decreased, comparing LiTFSI in PC electrolyte cells, one self-mixed in situ and three operando cells, two using self-mixed electrolytes of different concentration and one with a commercial electrolyte. For both protocols, the detailed scans were taken 15 min after the voltage was swept but the electrodes of the operando cells were pulled up from the electrolyte bath before the voltage sweep. A guide to the eye is included in the figure, indicating a slope of 1 eV/V.

As in Paper I, an expected behaviour of KE energy shifts as a function of constant voltage is a (near) 1 eV/V slope until approximately 0.5 V, where intercalation of the GC leads to a lower slope. Two cells deviate from the expected trend, most notably the operando cell containing 0.5 M self-mixed LiTFSI electrolyte, where increasingly large deviations emerge at lower voltages. For this cell, a GC signal is visible in all spectra at 1515.5 eV (Figure 6.1b) indicating that a thin meniscus is being probed. Notably, between OCV and 2 V, where the spectra most closely follow the 1 eV/V trend, the relative electrolyte peak intensity compared to the GC peak, is higher, indicating a slightly thicker meniscus than for lower voltages. The operando cell with 1.0 M self-mixed LiTFSI also shows deviations, though mostly in the 1.1-0.7 V range. Surprisingly, between 2.5 V and 1.1 V where a small GC peak can be seen in the spectra (Figure 6.4c), the cell follows the trend quite well despite the thin meniscus. At these voltages however, as shown in the current data of Paper I, the current is low as it is before the onset of SEI and the main contribution is the decomposition of impurities. Therefore deviations from 1 eV/V due to iR-drops in the meniscus are expected to be small.

The two remaining cells, the in situ self-mixed 1.0 M electrolyte and the operando

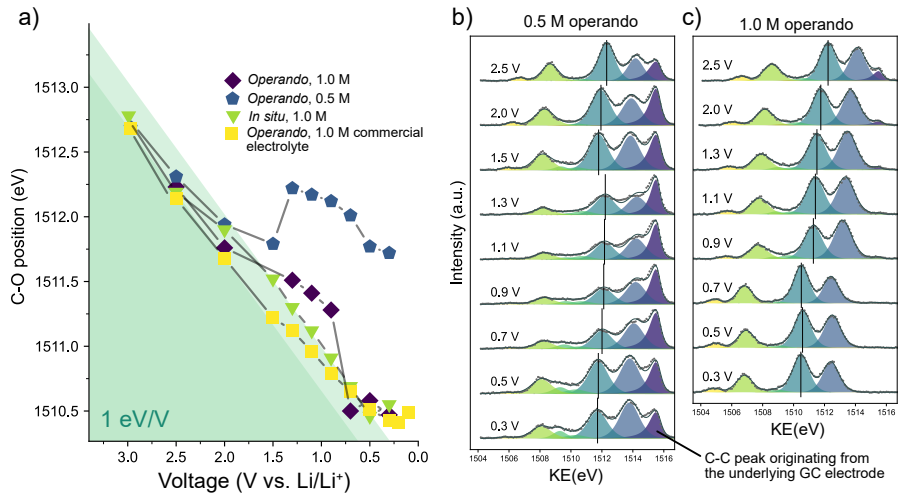

Figure 6.4: a) The kinetic energy position of the C-O peaks as a function of constant applied voltage, comparing data from both cells cycled in situ and operando and higher (1.0 M) and lower (0.5 M) concentration electrolytes. b) Fitted C1s spectra of the self-mixed 0.5 M electrolyte cell and c) of the self-mixed 1.0 M electrolyte cell, both cycled with the operando protocol. The vertical lines show the position of the C-O peak, which is plotted in a).

commercial 1.0 M electrolyte, follow the expected trend more consistently across the probed voltage range. While the spectra are not included here but shown in Paper II, no GC signals were detected in any of the spectra of these two cells. Overall, measurements obtained with thinner electrolyte films, where the electrode's GC signal becomes visible, show greater scatter and reduced reliability, suggesting that such conditions warrant caution. Nevertheless, subtle deviations are observed in the voltage window between 2.5 and 0.7 V for the in situ and operando commercial electrolyte cells despite no GC peaks being visible. The in situ cell deviates slightly from the 1 eV/V trend at higher voltages before recovering below ∼1.5 V, a behaviour which in Paper I was discussed to be due to reactions involving minority species. In contrast, the operando commercial electrolyte cell follows the ideal trend down to ∼1.5 V before the slope decreases. Disregarding the electrolyte composition, which in Paper II did not appear to influence this behaviour for the in situ protocol, the primary differences between the in situ and operando protocols are (i) the duration for which the electrodes are in a pulled-up state and (ii) the position of the WE as the voltage is applied. In the operando configuration, the voltage is applied across a thin and potentially drying meniscus, making iR-drops more significant, particularly as the current increases during SEI formation. This could therefore explain the deviation from 1.5 V and forward, an effect that was not observed for the in situ cell. Contrarily, in the 2.5-1.5 V region where the in situ cell showed a deviation but the operando did not, it could be possible that for the operando cell the minority-driven reactions are suppressed due to the iR-drop causing an lower effective voltage in the meniscus,

reducing the driving force for such reactions. Therefore, no deviation would be seen as currents are very small.

6.2.2 Factors affecting meniscus stability

From Figure 6.4a, it can be seen that out of the operando cells, the commercial electrolyte behaved most like the in situ cell and followed the expected trend more closely. A reason for this might be the quality of the meniscus. Images showing the electrolyte meniscus of a 1.0 M self-mixed electrolyte cell at the end of cycling can be seen in 6.5a. An image of the corresponding commercial 1.0 M electrolyte meniscus can be seen in Figure 6.5b. With the self-mixed electrolyte, small particles are visible on the surface, which we attribute to salt crystals. These visible salt crystals were only detected after the electrodes had been dipped multiple times and were not present in all self-mixed electrolyte menisci examined. In contrast, however, no particles are observed for the commercial electrolyte at any stage during the experiment. We therefore emphasise the importance of thorough mixing and maintaining clean conditions to minimize dust and particle contamination to achieve a reliable meniscus. In addition, solvent evaporation may be enhanced by the differential pumping of the analyser nozzle, which affects an area much larger than the X-ray beam itself and can lead to localised drying when the electrode remains stationary. Images of these effects can be seen in Figure 6.5c and 6.5d. We therefore recommend that detailed scans also be performed under continuous electrode motion to minimise meniscus drying and that when not measuring, the analyser nozzle is kept away from the meniscus area to be probed.

6.2.3 Mass transport in the meniscus

For the two cells that deviated most strongly from the expected 1 eV/V behaviour, the self-mixed 1.0 M operando and self-mixed 0.5 M operando cells, time-resolved measurements as the cells are stepped to 2.5 V, 1.3 V and 0.3 V are shown together with the corresponding current response in Figure 6.6. Any differences in the response of the KE positions compared to the current response, measured between WE and CE, would mean that mass transport differs between the meniscus and the bulk electrolyte in the cell, meaning there is increased resistance in the meniscus leading to an iR-drop.

For the 1.0 M electrolyte, the time-resolved measurements show very close agreement between the electrochemical current and the shifts in KE, with no detectable delay for any applied voltage step. This indicates that mass transport limitations and iR-drops in the meniscus are negligible under these conditions. The freshly formed meniscus is expected to be relatively thick, and drying effects are minimal compared to those observed during detailed scans. Only a minor deviation is observed near 1.3 V, which is attributed to local meniscus inhomogeneities such as salt crystals or other debris as discussed previously. In contrast, the 0.5 M electrolyte exhibits a delayed KE response relative to the current at 2.5 V suggesting the presence of an iR-drop and sluggish mass transport within the meniscus even though the electrodes were pulled just seconds before the start

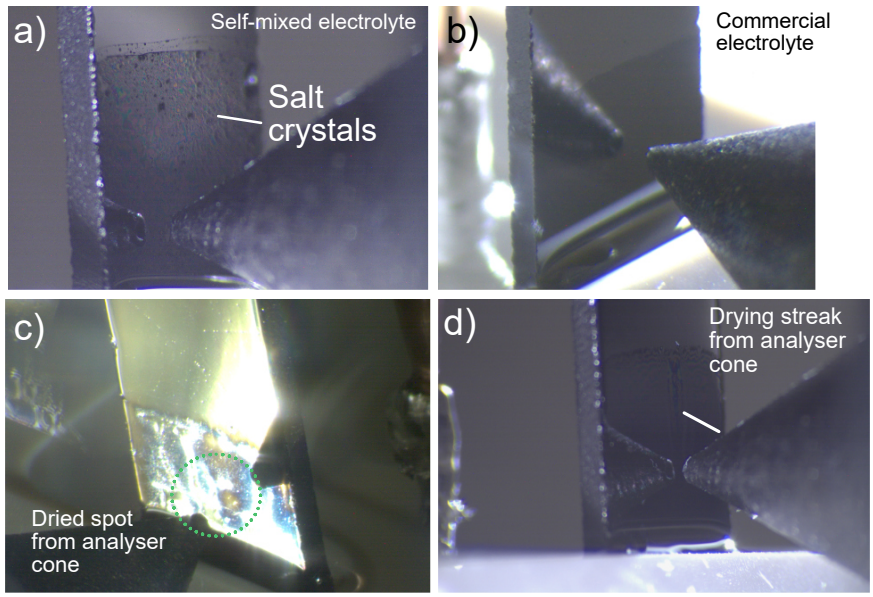

Figure 6.5: a) A photograph of a GC electrode pulled up from a self-mixed electrolyte cell in front the analyser nozzle. Some small particles of what is believed to be salt crystals can be seen. b) A photograph of a GC electrode pulled up from the commercial where no particles can be seen. c) The differential pumping between the analysis chamber and the electron analyser will cause vapour to be pumped out through the analyser cone. When the electrodes were left up for longer amounts of time, a dried spot could be seen on the electrode. d) The drying effect of the cone could sometimes be seen when the electrodes were pulled up, leaving a visible streak in the meniscus.

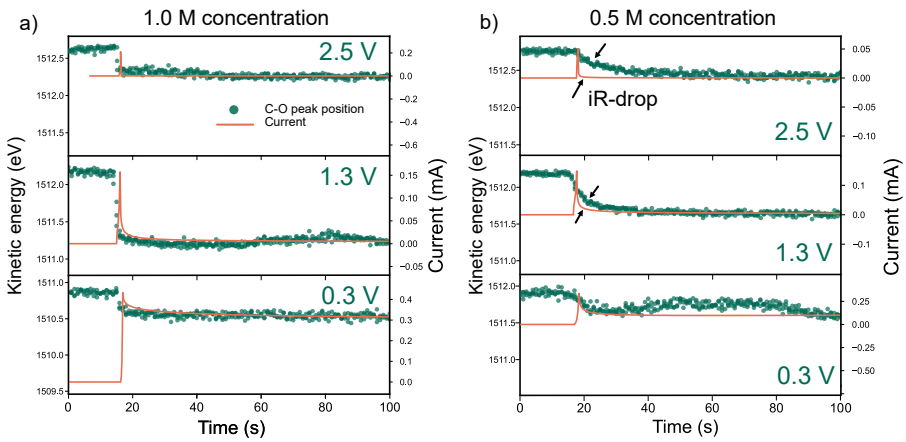

Figure 6.6: The cell current and time resolved C-O peak position measured as the cell is stepped to a new constant voltage, for a) the self-mixed 1.0 M electrolyte and b) the self-mixed 0.5 M electrolyte.

of the time-resolved measurement. At the two lower voltage steps, the delay between current and KE data is however smaller. This behaviour is unexpected, as the cell current increases for lower voltages and larger iR-drops and stronger mass-transport limitations would normally be anticipated. The detailed scans for this cell recorded after the time-resolved measurements (Figure 6.4a and b) showed deviations from the ideal 1 eV/V trend and revealed a GC signal, indicating a thin or drying meniscus that could hinder ion transport. Despite these indications, clear iR-drop-related delays are not observed at lower voltages. Additionally, the KE shifts for the 0.5 M electrolyte are smaller than those for the 1.0 M electrolyte at comparable voltages, suggesting that mechanisms beyond iR-drops contribute to the deviations. Increased noise and and bumps in the KE data shown for the 0.3 V voltage sweep could stem from salt crystals or debris, though the exact origin remains unclear.

Overall, these results highlight the importance of time-resolved measurements, which provide insights beyond the detailed scans and help distinguish between iR-drop effects and other interfacial processes. It is therefore beneficial to employ both in situ and operando approaches: first to compare detailed steady state scans, and subsequently to use time-resolved operando measurements to rule out iR-drops as the origin of the observed deviations, further strengthening hypotheses about 1 eV/V deviations.

Chapter 7
Conclusions and outlook

This thesis discusses the dip-and-pull method of ambient-pressure X-ray photoelectron spectroscopy and its application to measurements of model lithium-ion battery systems. In this concluding chapter, I summarise the main results and conclusions from Paper I and Paper II, place them in context from my own perspective, and discuss experiments that I consider particularly interesting to pursue in order to move the science forward.

A technique based on self-discharge and relaxation of the EDL has been developed that enables detecting the onset of SEI formation on the negative electrode. Previously, this has not been possible using APXPS measurements of a thick electrolyte meniscus. By applying time-resolved measurements, more detailed insight into the kinetics at the electrode/electrolyte interface can be obtained, even without directly probing the underlying electrode. The results show that SEI formation passivates the carbon negative electrode and suppresses parasitic reactions at the electrode surface. With an improved understanding of the different kinetic regimes of the electrode/electrolyte interface, deviations from the expected 1 eV/V relationship between shifted electrolyte peaks and the applied voltage can be analysed in greater detail.

We proposed a hypothesis that the electron chemical potential in the meniscus cannot always be treated as constant when interfacial reactions are strongly influenced by minority species in the electrolyte. This situation may occur at voltages where the main electrolyte components, salt and solvent, have not yet begun to undergo reduction to form an SEI. This hypothesis is used to explain small deviations from the expected 1 eV/V relationship that cannot be accounted for by simple iR-drops in the meniscus. However, no chemical analysis has been performed to determine how large the concentration of such impurities would need to be for this effect to become significant. It therefore remains unclear whether consumption of minority species would noticeably alter the overall electron chemical potential. Future work could investigate systems with controlled amounts of impurity species, such as water, and correlate these concentrations with the extent of SEI formation at different stages. It should also be noted that the overall electrolyte volume in the APXPS electrochemical cells is large and only a small fraction of that is present in the meniscus, which may lead to locally different concentrations compared to the bulk electrolyte.

To better understand how meniscus thickness, stability, and electrode position influence kinetic energy shifts and electrochemical potentials, experiments were also performed comparing operando and in situ measurement protocols. These protocols differed in the time that the electrodes were pulled from the electrolyte and if the electrodes were in the pulled state when the voltage was applied. The results show that thinner menisci are associated with less reliable measurements, consistent with previous expectations [112]. In addition, and less well understood,

is the observation that iR-drops may not always be the main cause of deviations from the 1 eV/V relationship in very thin menisci. I believe that iR-drops have often been the most convenient explanation for such deviations. However, time-resolved measurement techniques enable a more nuanced analysis of these effects. The papers included in this thesis clarify the available experimental options for APXPS measurements on battery systems and aim to assist researchers in selecting dip-and-pull methods that best match their specific research questions. Potential challenges associated with probing thin menisci are also identified, along with strategies to mitigate these issues through appropriate electrolyte selection and measurement design.

As a final outlook, since the measurements presented here probe the thick electrolyte well outside of the electric double layer, the exact shape of the electrostatic potential profile remains unknown. The original motivation for introducing the voltage relaxation approach was to investigate the evolution of the potential profile as the SEI was formed on the electrode, and which effects that could potentially have on the kinetics of the chemical reactions. Although this was not achieved in the present work, I remain interested in whether the technique still could be used to detect the profile and if the same electrochemical potential gradients, measured to exist between the SEI and electrode in post-mortem XPS measurements on graphite electrodes [6, 81], can still be measured when electrolytes are present. One possible experiment could involve intentionally drying the meniscus, gradually exposing and probing the SEI. Perhaps this could provide insight into how this layer influences electrochemical potentials at the interface. It would also be valuable to model electrochemical potentials using molecular dynamics and density functional theory and to connect these simulations with APXPS measurements. Such combined approaches may help predict how spectral peaks are expected to shift under different applied voltages and enable more detailed peak analysis.

Acknowledgements

A battery without an SEI is a very bad battery, which would decompose before accomplishing anything. The same can be said about a PhD student without her supervisors and colleagues.

First and foremost I would like to thank Julia Maibach for being such an inspiring and supporting supervisor, and for putting up with my obsession of working close to deadlines and drawing near incomprehensible scribbles on all of her office whiteboards. I would also like to thank my co-supervisors Patrik Johansson and Joakim Halldin Stenlid who were both thrown in to my project late but has shown nothing but enthusiasm and support. Thank you also to my examiner and great big boss Aleksandar Matic, for having (or at least saying that he has) great faith in my capabilities as a researcher, even when I feel like the opposite.

A big thank you also goes out to everyone who participated in the beamtimes of this work, Auðunn, Isak, Simon, Hanna and Gritt. Without this data it would be a very thin thesis indeed. Thank you also to Rob Temperton, beamline scientist at HIPPIE, for assisting us with all of the measurements. In the home lab, Ezio Zanghellini deserves a special recognition and a thank you for handling all of my (sometimes less intelligent) questions about lab equipment and experiments.

Elin, my evil twin and partner in crime, you know what you have done. Isak, thank you for being a great friend and for helping me with my code, but mostly for the friend thing. Quan and Marita, you are the absolute best office mates a girl could hope for. To the rest of my MF colleagues: without having any empirical evidence I would still confidently say that we are the best research group in the world. Thank you. You are all amazing people.

Finally, I need to thank my family, friends, football teammates in IK Virgo and especially Tim for supporting me during these first years of my PhD. Without you I would have crashed and burned long ago.

Bibliography

[1] K. Xu, *Electrolytes, Interfaces and Interphases: Fundamentals and Applications in Batteries*. Royal Society of Chemistry, Apr. 2023.

[2] E. Peled, 'The Electrochemical Behavior of Alkali and Alkaline Earth Metals in Nonaqueous Battery Systems—The Solid Electrolyte Interphase Model,' *Journal of The Electrochemical Society*, vol. 126, no. 12, p. 2047, Dec. 1979. DOI: 10.1149/1.2128859.

[3] P. M. Attia, S. Das, S. J. Harris, M. Z. Bazant and W. C. Chueh, 'Electrochemical Kinetics of SEI Growth on Carbon Black: Part I. Experiments,' *Journal of The Electrochemical Society*, vol. 166, no. 4, E97, Feb. 2019. DOI: 10.1149/2.0231904jes.

[4] Q. Fang et al., 'Interfacial degradation of silicon anodes in pouch cells,' *Energy & Environmental Science*, vol. 17, no. 17, pp. 6368–6376, Aug. 2024. DOI: 10.1039/D4EE01755B.

[5] M. Hao, S. Weng, C. Zhong, Y. Li and X. Wang, 'Structure and evolution of solid electrolyte interphase (SEI) at the electrode-electrolyte interface,' *Materials Today Energy*, vol. 53, p. 101 998, Oct. 2025. DOI: 10.1016/j.mtener.2025.101998.

[6] F. Lindgren et al., 'Breaking Down a Complex System: Interpreting PES Peak Positions for Cycled Li-Ion Battery Electrodes,' *The Journal of Physical Chemistry C*, vol. 121, no. 49, pp. 27 303–27 312, Dec. 2017. DOI: 10.1021/acs.jpcc.7b08923.

[7] S. Oswald, M. Hoffmann and M. Zier, 'Peak position differences observed during XPS sputter depth profiling of the SEI on lithiated and delithiated carbon-based anode material for Li-ion batteries,' *Applied Surface Science*, vol. 401, pp. 408–413, Apr. 2017. DOI: 10.1016/j.apsusc.2016.12.223.

[8] I. Källquist et al., 'Probing Electrochemical Potential Differences over the Solid/Liquid Interface in Li-Ion Battery Model Systems,' *ACS Applied Materials & Interfaces*, vol. 13, no. 28, pp. 32 989–32 996, Jul. 2021. DOI: 10.1021/acsami.1c07424.

[9] I. Källquist et al., 'Potentials in Li-Ion Batteries Probed by Operando Ambient Pressure Photoelectron Spectroscopy,' *ACS Applied Materials & Interfaces*, vol. 14, no. 5, pp. 6465–6475, Feb. 2022. DOI: 10.1021/acsami.1c12465.

[10] J. O. Bockris and A. K. N. Reddy, *Modern Electrochemistry: Volume 2*. Boston, MA: Springer US, 1973. DOI: 10.1007/978-1-4613-4560-2.

[11] K. Xu, 'Electrolytes and Interphases in Li-Ion Batteries and Beyond,' *Chemical Reviews*, vol. 114, no. 23, pp. 11 503–11 618, Dec. 2014. DOI: 10.1021/cr500003w.

[12] J. Koryta, J. Dvorak and L. Kavan, *Principles of Electrochemistry*. Wiley, Apr. 1993.

[13] X. Chen, X.-Q. Zhang, H.-R. Li and Q. Zhang, 'Cation-Solvent, Cation-Anion, and Solvent-Solvent Interactions with Electrolyte Solvation in Lithium Batteries,' *Batteries & Supercaps*, vol. 2, no. 2, pp. 128–131, 2019. DOI: 10.1002/batt.201800118.

[14] R. A. Miranda-Quintana and J. Smiatek, 'Beneficial properties of solvents and ions for lithium ion and post-lithium ion batteries: Implications from charge transfer models,' *Electrochimica Acta*, vol. 384, p. 138 418, Jul. 2021. DOI: 10.1016/j.electacta.2021.138418.

[15] D. M. Seo et al., 'Role of Mixed Solvation and Ion Pairing in the Solution Structure of Lithium Ion Battery Electrolytes,' *The Journal of Physical Chemistry C*, vol. 119, no. 25, pp. 14 038–14 046, Jun. 2015. DOI: 10.1021/acs.jpcc.5b03694.

[16] D. K. Cheng, *Field and Wave Electromagnetics*. Pearson, 2014.

[17] A. J. Bard and L. R. Faulkner, *Electrochemical Methods : Fundamentals and Applications*. John Wiley & Sons, 1980.

[18] S. W. Boettcher et al., 'Potentially Confusing: Potentials in Electrochemistry,' *ACS Energy Letters*, vol. 6, no. 1, pp. 261–266, Jan. 2021. DOI: 10.1021/acsenergylett.0c02443.

[19] H. Helmholtz, 'Ueber einige Gesetze der Vertheilung elektrischer Ströme in körperlichen Leitern mit Anwendung auf die thierisch-elektrischen Versuche,' *Annalen der Physik*, vol. 165, no. 6, pp. 211–233, 1853. DOI: 10.1002/andp.18531650603.

[20] J. Perrin, 'Mécanisme de l'électrisation de contact et solutions colloïdales,' *Journal de Chimie Physique*, vol. 2, pp. 601–651, 1904. DOI: 10.1051/jcp/1904020601.

[21] V. D. Ivanov, 'The Helmholtz model,' *Journal of Solid State Electrochemistry*, vol. 28, no. 8, pp. 2487–2493, Aug. 2024. DOI: 10.1007/s10008-024-05850-5.

[22] M. Gouy, 'Sur la constitution de la charge électrique à la surface d'un électrolyte,' *Journal de Physique Théorique et Appliquée*, vol. 9, no. 1, pp. 457–468, 1910. DOI: 10.1051/jphystap:019100090045700.

[23] D. L. Chapman, 'A contribution to the theory of electrocapillarity,' *The London, Edinburgh, and Dublin Philosophical Magazine and Journal of Science*, vol. 25, no. 148, pp. 475–481, Apr. 1913. DOI: 10.1080/14786440408634187.

[24] O. Stern, 'Zur Theorie Der Elektrolytischen Doppelschicht,' *Zeitschrift für Elektrochemie und angewandte physikalische Chemie*, vol. 30, no. 21-22, pp. 508–516, 1924. DOI: 10.1002/bbpc.192400182.

[25] D. C. Grahame, 'The Electrical Double Layer and the Theory of Electrocapillarity.,' *Chemical Reviews*, vol. 41, no. 3, pp. 441–501, Dec. 1947. DOI: 10.1021/cr60130a002.

[26] J. O. Bockris, M. A. V. Devanathan and K. Müller, 'On the structure of charged interfaces,' *Proceedings of the Royal Society of London. A. Mathematical and Physical Sciences*, vol. 274, no. 1356, pp. 55–79, Jun. 1963. DOI: 10.1098/rspa.1963.0114.

[27] X. Chen, N. Yao, Z. Zheng, Y.-C. Gao and Q. Zhang, 'A perspective on the fundamental theory of nonaqueous electrolytes for rechargeable batteries,' *National Science Review*, vol. 12, no. 7, Jun. 2025. DOI: 10.1093/nsr/nwae394.

[28] L. Chen et al., 'Dynamic shielding of electrified interface enables high-voltage lithium batteries,' *Chem*, vol. 10, no. 4, pp. 1196–1212, Apr. 2024. DOI: 10.1016/j.chempr.2024.01.001.

[29] Q. Wu and Y. Qi, 'Revealing heterogeneous electric double layer (EDL) structures of localized high-concentration electrolytes (LHCEs) and their impact on solid–electrolyte interphase (SEI) formation in lithium batteries,' *Energy & Environmental Science*, vol. 18, no. 6, pp. 3036–3046, Mar. 2025. DOI: 10.1039/D5EE00206K.

[30] C. Tozzi et al., 'Electric Double Layer and Structure of the Li-ion Battery Separator/Liquid Electrolyte Interface Detected with the Atomic Force Microscope,' *The Journal of Physical Chemistry C*, vol. 128, no. 43, pp. 18 182–18 190, Oct. 2024. DOI: 10.1021/acs.jpcc.4c04758.

[31] J. O. Bockris and A. K. N. Reddy, *Modern Electrochemistry: Volume 1*. Boston, MA: Springer US, 1970. DOI: 10.1007/978-1-4615-8600-5.

[32] A. W. Colburn, K. J. Levey, D. O'Hare and J. V. Macpherson, 'Lifting the lid on the potentiostat: A beginner's guide to understanding electrochemical circuitry and practical operation,' *Physical Chemistry Chemical Physics*, vol. 23, no. 14, pp. 8100–8117, Apr. 2021. DOI: 10.1039/D1CP00661D.

[33] K. W. Beard, Ed., *Linden's Handbook of Batteries*, 5th Edition. McGraw-Hill Education, 2019.

[34] S. Clark et al., 'Toward a Unified Description of Battery Data,' *Advanced Energy Materials*, vol. 12, no. 17, p. 2 102 702, 2022. DOI: 10.1002/aenm.202102702.

[35] G. N. Lewis and F. G. Keyes, 'The potential of the lithium electrode,' *Journal of the American Chemical Society*, vol. 35, no. 4, pp. 340–344, Apr. 1913. DOI: 10.1021/ja02193a004.

[36] A. Groß and S. Sakong, 'Modelling the electric double layer at electrode/electrolyte interfaces,' *Current Opinion in Electrochemistry*, Bioelectrochemistry Electrocatalysis, vol. 14, pp. 1–6, Apr. 2019. DOI: 10.1016/j.coelec.2018.09.005.

[37] J. B. Goodenough and K.-S. Park, 'The Li-Ion Rechargeable Battery: A Perspective,' *Journal of the American Chemical Society*, vol. 135, no. 4, pp. 1167–1176, Jan. 2013. DOI: 10.1021/ja3091438.

[38] M. Yoshio, R. J. Brodd and A. Kozawa, Eds., *Lithium-Ion Batteries: Science and Technologies*. New York, NY: Springer, 2009. DOI: 10.1007/978-0-387-34445-4.

[39] D. Aurbach, B. Markovsky, A. Shechter, Y. Ein-Eli and H. Cohen, 'A Comparative Study of Synthetic Graphite and Li Electrodes in Electrolyte Solutions Based on Ethylene Carbonate-Dimethyl Carbonate Mixtures,' *Journal of The Electrochemical Society*, vol. 143, no. 12, p. 3809, Dec. 1996. DOI: 10.1149/1.1837300.

[40] D. Aurbach, 'Review of selected electrode–solution interactions which determine the performance of Li and Li ion batteries,' *Journal of Power Sources*, vol. 89, no. 2, pp. 206–218, Aug. 2000. DOI: 10.1016/S0378-7753(00)00431-6.

[41] K. Xu, 'Nonaqueous Liquid Electrolytes for Lithium-Based Rechargeable Batteries,' *Chemical Reviews*, vol. 104, no. 10, pp. 4303–4418, Oct. 2004. DOI: 10.1021/cr030203g.

[42] M. Sadd, S. Xiong, J. R. Bowen, F. Marone and A. Matic, 'Investigating microstructure evolution of lithium metal during plating and stripping via operando X-ray tomographic microscopy,' *Nature Communications*, vol. 14, no. 1, p. 854, Feb. 2023. DOI: 10.1038/s41467-023-36568-z.

[43] X. Zhang, A. Wang, X. Liu and J. Luo, 'Dendrites in Lithium Metal Anodes: Suppression, Regulation, and Elimination,' *Accounts of Chemical Research*, vol. 52, no. 11, pp. 3223–3232, Nov. 2019. DOI: 10.1021/acs.accounts.9b00437.

[44] M. B. Armand, 'Intercalation Electrodes,' in *Materials for Advanced Batteries*, D. W. Murphy, J. Broadhead and B. C. H. Steele, Eds., Boston, MA: Springer US, 1980, pp. 145–161. DOI: 10.1007/978-1-4684-3851-2_7.

[45] P. Li, H. Kim, S.-T. Myung and Y.-K. Sun, 'Diverting Exploration of Silicon Anode into Practical Way: A Review Focused on Silicon-Graphite Composite for Lithium Ion Batteries,' *Energy Storage Materials*, vol. 35, pp. 550–576, Mar. 2021. DOI: 10.1016/j.ensm.2020.11.028.

[46] H. Dong et al., 'Exploring the practical applications of silicon anodes: A review of silicon-based composites for lithium-ion batteries,' *Ionics*, vol. 28, Jul. 2022. DOI: 10.1007/s11581-022-04622-3.

[47] J. C. Stallard et al., 'Mechanical properties of cathode materials for lithium-ion batteries,' *Joule*, vol. 6, no. 5, pp. 984–1007, May 2022. DOI: 10.1016/j.joule.2022.04.001.

[48] J. Xiang et al., 'Building Practical High-Voltage Cathode Materials for Lithium-Ion Batteries,' *Advanced Materials*, vol. 34, no. 52, p. 2 200 912, 2022. DOI: 10.1002/adma.202200912.

[49] C. Liu, Z. G. Neale and G. Cao, 'Understanding electrochemical potentials of cathode materials in rechargeable batteries,' *Materials Today*, vol. 19, no. 2, pp. 109–123, Mar. 2016. DOI: 10.1016/j.mattod.2015.10.009.

[50] R. Malik, A. Abdellahi and G. Ceder, 'A Critical Review of the Li Insertion Mechanisms in LiFePO4 Electrodes,' *Journal of The Electrochemical Society*, vol. 160, no. 5, A3179, May 2013. DOI: 10.1149/2.029305jes.

[51] L.-X. Yuan et al., 'Development and challenges of LiFePO4 cathode material for lithium-ion batteries,' *Energy & Environmental Science*, vol. 4, no. 2, pp. 269–284, Feb. 2011. DOI: 10.1039/C0EE00029A.

[52] F. La Mantia, C. D. Wessells, H. D. Deshazer and Y. Cui, 'Reliable reference electrodes for lithium-ion batteries,' *Electrochemistry Communications*, vol. 31, pp. 141–144, Jun. 2013. DOI: 10.1016/j.elecom.2013.03.015.

[53] M. D. Levi, V. Dargel, Y. Shilina, D. Aurbach and I. C. Halalay, 'Impedance Spectra of Energy-Storage Electrodes Obtained with Commercial Three-Electrode Cells: Some Sources of Measurement Artefacts,' *Electrochimica Acta*, vol. 149, pp. 126–135, Dec. 2014. DOI: 10.1016/j.electacta.2014.10.083.

[54] D. Rutz, I. Bauer, F. Brauchle and T. Jacob, 'Designing a reference electrode – An approach to fabricate laser perforated reference electrodes for lithium-ion batteries,' *Electrochimica Acta*, vol. 441, p. 141 768, Feb. 2023. DOI: 10.1016/j.electacta.2022.141768.

[55] R. Fong, U. v. Sacken and J. R. Dahn, 'Studies of Lithium Intercalation into Carbons Using Nonaqueous Electrochemical Cells,' *Journal of The Electrochemical Society*, vol. 137, no. 7, p. 2009, Jul. 1990. DOI: 10.1149/1.2086855.

[56] J. Li et al., 'An Artificial Solid Electrolyte Interphase Enables the Use of a LiNi0.5 Mn1.5 O4 5 V Cathode with Conventional Electrolytes,' *Advanced Energy Materials*, vol. 3, no. 10, pp. 1275–1278, 2013. DOI: 10.1002/aenm201300378.

[57] Y. Qian et al., 'Influence of electrolyte additives on the cathode electrolyte interphase (CEI) formation on LiNi1/3Mn1/3Co1/3O2 in half cells with Li metal counter electrode,' *Journal of Power Sources*, vol. 329, pp. 31–40, Oct. 2016. DOI: 10.1016/j.jpowsour.2016.08.023.

[58] S. P. Kühn, K. Edström, M. Winter and I. Cekic-Laskovic, 'Face to Face at the Cathode Electrolyte Interphase: From Interface Features to Interphase Formation and Dynamics,' *Advanced Materials Interfaces*, vol. 9, no. 8, p. 2 102 078, DOI: 10.1002/admi.202102078.

[59] B. Heidrich, L. Pritzlaff, M. Börner, M. Winter and P. Niehoff, 'Comparative X-ray Photoelectron Spectroscopy Study of the SEI and CEI in Three Different Lithium Ion Cell Formats,' *Journal of The Electrochemical Society*, vol. 169, no. 3, p. 030 533, Mar. 2022. DOI: 10.1149/1945-7111/ac5c08.

[60] S. Malmgren et al., 'Comparing anode and cathode electrode/electrolyte interface composition and morphology using soft and hard X-ray photoelectron spectroscopy,' *Electrochimica Acta*, vol. 97, pp. 23–32, May 2013. DOI: 10.1016/j.electacta.2013.03.010.

[61] G. V. Zhuang, K. Xu, H. Yang, T. R. Jow and P. N. Ross, 'Lithium ethylene dicarbonate identified as the primary product of chemical and electrochemical reduction of EC in 1.2 M LiPF6/EC:EMC electrolyte,' *The Journal of Physical Chemistry. B*, vol. 109, no. 37, pp. 17 567–17 573, Sep. 2005. DOI: 10.1021/jp052474w.

[62] K. Xu, Y. Lam, S. S. Zhang, T. R. Jow and T. B. Curtis, 'Solvation Sheath of Li+ in Nonaqueous Electrolytes and Its Implication of Graphite/Electrolyte Interface Chemistry,' *The Journal of Physical Chemistry C*, vol. 111, no. 20, pp. 7411–7421, May 2007. DOI: 10.1021/jp068691u.

[63] K. Xu, 'Whether EC and PC Differ in Interphasial Chemistry on Graphitic Anode and How,' *Journal of The Electrochemical Society*, vol. 156, no. 9, A751, Jul. 2009. DOI: 10.1149/1.3166182.

[64] L. Xing et al., 'Deciphering the Ethylene Carbonate–Propylene Carbonate Mystery in Li-Ion Batteries,' *Accounts of Chemical Research*, vol. 51, no. 2, pp. 282–289, Feb. 2018. DOI: 10.1021/acs.accounts.7b00474.

[65] G. G. Eshetu et al., 'Impact of the electrolyte salt anion on the solid electrolyte interphase formation in sodium ion batteries,' *Nano Energy*, vol. 55, pp. 327–340, Jan. 2019. DOI: 10.1016/j.nanoen.2018.10.040.

[66] S. E. Sloop, J. K. Pugh, S. Wang, J. B. Kerr and K. Kinoshita, 'Chemical Reactivity of PF 5 and LiPF6 in Ethylene Carbonate/Dimethyl Carbonate Solutions,' *Electrochemical and Solid-State Letters*, vol. 4, no. 4, A42, Feb. 2001. DOI: 10.1149/1.1353158.

[67] D. Aurbach, M. L. Daroux, P. W. Faguy and E. Yeager, 'Identification of Surface Films Formed on Lithium in Propylene Carbonate Solutions,' *Journal of The Electrochemical Society*, vol. 134, no. 7, p. 1611, Jul. 1987. DOI: 10.1149/1.2100722.

[68] D. Aurbach et al., 'New insights into the interactions between electrode materials and electrolyte solutions for advanced nonaqueous batteries,' *Journal of Power Sources*, vol. 81-82, pp. 95–111, Sep. 1999. DOI: 10.1016/S0378-7753(99)00187-1.

[69] K. Edström, M. Herstedt and D. P. Abraham, 'A new look at the solid electrolyte interphase on graphite anodes in Li-ion batteries,' *Journal of Power Sources*, Selected papers presented at the 2004 Meeting of the International Battery Association, vol. 153, no. 2, pp. 380–384, Feb. 2006. DOI: 10.1016/j.jpowsour.2005.05.062.

[70] M. Nie et al., 'Lithium Ion Battery Graphite Solid Electrolyte Interphase Revealed by Microscopy and Spectroscopy,' *The Journal of Physical Chemistry C*, vol. 117, no. 3, pp. 1257–1267, Jan. 2013. DOI: 10.1021/jp3118055.

[71] S. K. Heiskanen, J. Kim and B. L. Lucht, 'Generation and Evolution of the Solid Electrolyte Interphase of Lithium-Ion Batteries,' *Joule*, vol. 3, no. 10, pp. 2322–2333, Oct. 2019. DOI: 10.1016/j.joule.2019.08.018.

[72] E. Peled, D. Golodnitsky and G. Ardel, 'Advanced Model for Solid Electrolyte Interphase Electrodes in Liquid and Polymer Electrolytes,' *Journal of The Electrochemical Society*, vol. 144, no. 8, p. L208, Aug. 1997. DOI: 10.1149/1.1837858.

[73] Y. Li et al., 'Correlating Structure and Function of Battery Interphases at Atomic Resolution Using Cryoelectron Microscopy,' *Joule*, vol. 2, no. 10, pp. 2167–2177, Oct. 2018. DOI: 10.1016/j.joule.2018.08.004.

[74] H. Adenusi, G. A. Chass, S. Passerini, K. V. Tian and G. Chen, 'Lithium Batteries and the Solid Electrolyte Interphase (SEI)—Progress and Outlook,' *Advanced Energy Materials*, vol. 13, no. 10, p. 2 203 307, 2023. DOI: 10.1002/aenm.202203307.

[75] O. Borodin et al., 'Modeling Insight into Battery Electrolyte Electrochemical Stability and Interfacial Structure,' *Accounts of Chemical Research*, vol. 50, no. 12, pp. 2886–2894, Dec. 2017. DOI: 10.1021/acs.accounts.7b00486.

[76] Y. Zhou et al., 'Real-time mass spectrometric characterization of the solid–electrolyte interphase of a lithium-ion battery,' *Nature Nanotechnology*, vol. 15, no. 3, pp. 224–230, Mar. 2020. DOI: 10.1038/s41565-019-0618-4.

[77] Y. Li and Y. Qi, 'Energy landscape of the charge transfer reaction at the complex Li/SEI/electrolyte interface,' *Energy & Environmental Science*, vol. 12, no. 4, pp. 1286–1295, Apr. 2019. DOI: 10.1039/C8EE03586E.

[78] N. Yao, X. Chen, Z.-H. Fu and Q. Zhang, 'Applying Classical, Ab Initio, and Machine-Learning Molecular Dynamics Simulations to the Liquid Electrolyte for Rechargeable Batteries,' *Chemical Reviews*, vol. 122, no. 12, pp. 10 970–11 021, Jun. 2022. DOI: 10.1021/acs.chemrev.1c00904.

[79] F. Chen, 'Atomistic modelling approaches to understanding the interfaces of ionic liquid electrolytes for batteries and electrochemical devices,' *Current Opinion in Electrochemistry*, vol. 35, p. 101 086, Oct. 2022. DOI: 10.1016/j.coelec.2022.101086.

[80] Q. Wu, M. T. McDowell and Y. Qi, 'Effect of the Electric Double Layer (EDL) in Multicomponent Electrolyte Reduction and Solid Electrolyte Interphase (SEI) Formation in Lithium Batteries,' *Journal of the American Chemical Society*, vol. 145, no. 4, pp. 2473–2484, Feb. 2023. DOI: 10.1021/jacs.2c11807.

[81] J. Maibach, F. Lindgren, H. Eriksson, K. Edström and M. Hahlin, 'Electric Potential Gradient at the Buried Interface between Lithium-Ion Battery Electrodes and the SEI Observed Using Photoelectron Spectroscopy,' *The Journal of Physical Chemistry Letters*, vol. 7, no. 10, pp. 1775–1780, May 2016. DOI: 10.1021/acs.jpclett.6b00391.

[82] J. Kim, F. Zhao, L. K. S. Bonagiri, Q. Ai and Y. Zhang, 'Electrical Double Layers Modulate the Growth of Solid–Electrolyte Interphases,' *Chemistry of Materials*, vol. 36, no. 19, pp. 9156–9166, Oct. 2024. DOI: 10.1021/acs.chemmater.4c01745.

[83] R. F. Ziesche et al., '4D imaging of lithium-batteries using correlative neutron and X-ray tomography with a virtual unrolling technique,' *Nature Communications*, vol. 11, no. 1, p. 777, Feb. 2020. DOI: 10.1038/s41467-019-13943-3.

[84] J. Maibach, J. Rizell, A. Matic and N. Mozhzhukhina, 'Toward Operando Characterization of Interphases in Batteries,' *ACS Materials Letters*, vol. 5, no. 9, pp. 2431–2444, Sep. 2023. DOI: 10.1021/acsmaterialslett.3c00207.

[85] A. Skurtveit et al., 'Operando X-Ray Diffraction and Total Scattering Characterization of Battery Materials: Not Just a Pretty Picture,' *Advanced Energy Materials*, vol. n/a, no. n/a, e06777, 2026. DOI: 10.1002/aenm.202506777.

[86] J. F. Watts and J. Wolstenholme, *An Introduction to Surface Analysis by XPS and AES*. Hoboken, NJ: Wiley, 2020.

[87] P. van der Heide, *X-Ray Photoelectron Spectroscopy: An Introduction to Principles and Practices*. Newark, UNITED STATES: John Wiley & Sons, Incorporated, 2011.

[88] F. A. Stevie and C. L. Donley, 'Introduction to x-ray photoelectron spectroscopy,' *Journal of Vacuum Science & Technology A: Vacuum, Surfaces, and Films*, vol. 38, no. 6, p. 063 204, Dec. 2020. DOI: 10.1116/6.0000412.

[89] G. H. Major et al., 'Practical guide for curve fitting in x-ray photoelectron spectroscopy,' *Journal of Vacuum Science & Technology A*, vol. 38, no. 6, p. 061 203, Oct. 2020. DOI: 10.1116/6.0000377.

[90] S. Hofmann, *Auger- and X-Ray Photoelectron Spectroscopy in Materials Science: A User-Oriented Guide* (Springer Series in Surface Sciences). Berlin, Heidelberg: Springer, 2013, vol. 49. DOI: 10.1007/978-3-642-27381-0.

[91] 'DA30-L-8000 - Scienta Omicron,' Accessed: 24th Apr. 2026. [Online]. Available: https://scientaomicron.com/en/Instruments/Electron-Analysers/DA30-L-8000.

[92] 'PHOIBOS 150 1D-DLD | Specs,' Accessed: 24th Apr. 2026. [Online]. Available: https://www.specs-group.com/specs/products/detail/phoibos-150-1d-dld/.

[93] D. E. Starr, 'A Brief Overview of the Principles of Ambient Pressure X-ray Spectroscopies,' in *Ambient Pressure Spectroscopy in Complex Chemical Environments*, ser. ACS Symposium Series 1396, vol. 1396, Section: 1, American Chemical Society, Nov. 2021, pp. 1–17. DOI: 10.1021/bk-2021-1396.ch001.

[94] B. Rotonnelli et al., 'Methodological insights into the dip-and-pull X-ray photoelectron spectroscopy technique: Analysing electrochemical interfaces under in situ/operando conditions,' *Journal of Synchrotron Radiation*, vol. 33, no. 1, pp. 130–141, Jan. 2026. DOI: 10.1107/S1600577525008811.

[95] S. Axnanda et al., 'Using "Tender" X-ray Ambient Pressure X-Ray Photoelectron Spectroscopy as A Direct Probe of Solid-Liquid Interface,' *Scientific Reports*, vol. 5, no. 1, p. 9788, May 2015. DOI: 10.1038/srep09788.

[96] M. F. Lichterman et al., 'Direct observation of the energetics at a semiconductor/liquid junction by operando X-ray photoelectron spectroscopy,' *Energy & Environmental Science*, vol. 8, no. 8, pp. 2409–2416, Jul. 2015. DOI: 10.1039/C5EE01014D.

[97] 'NAP XPS Systems - Pressures up to 100 mbar | SPECS,' Accessed: 24th Apr. 2026. [Online]. Available: https://www.specs-group.com/specsgroup/knowledge/applications/productlines/detail/nap-xps-systems/.

[98] 'HiPP Lab - Scienta Omicron,' Accessed: 24th Apr. 2026. [Online]. Available: https://scientaomicron.com/HiPP-Lab.

[99] S. Zhu et al., 'HIPPIE: A new platform for ambient-pressure X-ray photoelectron spectroscopy at the MAX IV Laboratory,' *Journal of Synchrotron Radiation*, vol. 28, no. 2, pp. 624–636, Mar. 2021. DOI: 10.1107/S160057752100103X.

[100] P. Amann et al., 'A high-pressure x-ray photoelectron spectroscopy instrument for studies of industrially relevant catalytic reactions at pressures of several bars,' *Review of Scientific Instruments*, vol. 90, no. 10, p. 103 102, Oct. 2019. DOI: 10.1063/1.5109321.

[101] A. Balerna and S. Mobilio, 'Introduction to Synchrotron Radiation,' in *Synchrotron Radiation: Basics, Methods and Applications*, S. Mobilio, F. Boscherini and C. Meneghini, Eds., Berlin, Heidelberg: Springer, 2015, pp. 3–28. DOI: 10.1007/978-3-642-55315-8_1.

[102] '3 GeV storage ring,' Accessed: 24th Apr. 2026. [Online]. Available: https://www.maxiv.lu.se/beamlines-accelerators/accelerators/3-gev-storage-ring/.

[103] M. Favaro et al., 'Unravelling the electrochemical double layer by direct probing of the solid/liquid interface,' *Nature Communications*, vol. 7, no. 1, p. 12 695, Aug. 2016. DOI: 10.1038/ncomms12695.

[104] H. Ali-Löytty et al., 'Ambient-Pressure XPS Study of a Ni–Fe Electrocatalyst for the Oxygen Evolution Reaction,' *The Journal of Physical Chemistry C*, vol. 120, no. 4, pp. 2247–2253, Feb. 2016. DOI: 10.1021/acs.jpcc.5b10931.

[105] J. Maibach et al., 'Probing a battery electrolyte drop with ambient pressure photoelectron spectroscopy,' *Nature Communications*, vol. 10, no. 1, p. 3080, Jul. 2019. DOI: 10.1038/s41467-019-10803-y.

[106] C. J. Powell and A. Jablonski, *NIST Electron Inelastic-Mean-Free-Path Database*, Dec. 2010.

[107] D. Aegerter et al., 'Evaluation of Dip-And-Pull Ambient Pressure X-ray Photoelectron Spectroscopy for Investigating Oxygen Evolution Reaction Electrocatalysts,' *ACS Applied Energy Materials*, vol. 8, no. 19, pp. 14 554–14 567, Oct. 2025. DOI: 10.1021/acsaem.5c02252.

[108] M. Favaro et al., 'An Operando Investigation of (Ni–Fe–Co–Ce)Ox System as Highly Efficient Electrocatalyst for Oxygen Evolution Reaction,' *ACS Catalysis*, vol. 7, no. 2, pp. 1248–1258, Feb. 2017. DOI: 10.1021/acscatal.6b03126.

[109] H. Su, Y. Ye, K.-J. Lee, J. Zeng and E. J. Crumlin, 'Probing the nickel corrosion phenomena in alkaline electrolyte using tender x-ray ambient pressure x-ray photoelectron spectroscopy,' *Journal of Physics D: Applied Physics*, vol. 54, no. 37, p. 374 001, Jul. 2021. DOI: 10.1088/1361-6463/ac09bb.

[110] A. Larsson et al., '*In situ* quantitative analysis of electrochemical oxide film development on metal surfaces using ambient pressure X-ray photoelectron spectroscopy: Industrial alloys,' *Applied Surface Science*, vol. 611, p. 155 714, Feb. 2023. DOI: 10.1016/j.apsusc.2022.155714.

[111] F. Giovanni Capone et al., 'Operando observation of the dynamic SEI formation on a carbonaceous electrode by Near-Ambient Pressure XPS,' *Energy & Environmental Science*, 2024. DOI: 10.1039/D3EE03228K.

[112] A. Križan et al., 'Impact of Mass Transport on Meniscus Electrochemistry Determined by Time-Resolved Operando X-ray Photoelectron Spectroscopy,' *Physical Chemistry Chemical Physics*, Mar. 2025. DOI: 10.1039/D5CP00168D.

[113] V. Uskoković, 'A historical review of glassy carbon: Synthesis, structure, properties and applications,' *Carbon Trends*, vol. 5, p. 100 116, Oct. 2021. DOI: 10.1016/j.cartre.2021.100116.

[114] A. Dekanski, J. Stevanović, R. Stevanović, B. Ž. Nikolić and V. M. Jovanović, 'Glassy carbon electrodes: I. Characterization and electrochemical activation,' *Carbon*, vol. 39, no. 8, pp. 1195–1205, Jul. 2001. DOI: 10.1016/S0008-6223(00)00228-1.

[115] S. Pérez-Villar, P. Lanz, H. Schneider and P. Novák, 'Characterization of a model solid electrolyte interphase/carbon interface by combined *in situ* Raman/Fourier transform infrared microscopy,' *Electrochimica Acta*, vol. 106, pp. 506–515, Sep. 2013. DOI: 10.1016/j.electacta.2013.05.124.

[116] G. Zampardi, F. L. Mantia and W. Schuhmann, 'Determination of the formation and range of stability of the SEI on glassy carbon by local electrochemistry,' *RSC Advances*, vol. 5, no. 39, pp. 31 166–31 171, Mar. 2015. DOI: 10.1039/C5RA02940F.

[117] Y. Wu, T. Okajima and T. Ohsaka, 'Lithium Intercalation into Graphene Ribbons of Glassy Carbon,' *International Journal of Electrochemical Science*, vol. 12, no. 2, pp. 1004–1013, Feb. 2017. DOI: 10.20964/2017.02.48.

[118] Q. Qian, Y. Yang and H. Shao, 'Solid electrolyte interphase formation by propylene carbonate reduction for lithium anode,' *Physical Chemistry Chemical Physics*, vol. 19, no. 42, pp. 28 772–28 780, Nov. 2017. DOI: 10.1039/C7CP04839D.

[119] D. Aurbach and H. Gottlieb, 'The electrochemical behavior of selected polar aprotic systems,' *Electrochimica Acta*, vol. 34, no. 2, pp. 141–156, Feb. 1989. DOI: 10.1016/0013-4686(89)87079-3.

[120] Y. Pan, G. Wang and B. L. Lucht, 'Cycling performance and surface analysis of Lithium bis(trifluoromethanesulfonyl)imide in propylene carbonate with graphite,' *Electrochimica Acta*, vol. 217, pp. 269–273, Nov. 2016. DOI: 10.1016/j.electacta.2016.09.080.

[121] L. E. Helseth, 'The self-discharging of supercapacitors interpreted in terms of a distribution of rate constants,' *Journal of Energy Storage*, vol. 34, p. 102 199, Feb. 2021. DOI: 10.1016/j.est.2020.102199.

[122] L. H. Hess et al., 'The role of diffusion processes in the self-discharge of electrochemical capacitors,' *Energy Storage Materials*, vol. 37, pp. 501–508, May 2021. DOI: 10.1016/j.ensm.2021.02.007.

[123] S. Fletcher et al., 'The modelling of carbon-based supercapacitors: Distributions of time constants and Pascal Equivalent Circuits,' *Journal of Power Sources*, vol. 345, pp. 247–253, Mar. 2017. DOI: 10.1016/j.jpowsour.2017.02.012.

[124] 'Material | HTW Germany,' Accessed: 22nd Apr. 2026. [Online]. Available: https://htw-germany.com/en/material.